Stormflow response and 'effective' hydraulic conductivity of a degraded tropical Imperata grassland catchment as evaluated with two infiltration models

Zhuo Cheng[1], Jun Zhang[2], Bofu Yu[3], Nick A Chappell[4], Ilja H.J. van Meerveld[5], and Leendert Adrian Bruijnzeel[6]

[1]Department of Geography, Beijing Normal University
[2]Institute of International Rivers and Eco-Security
[3]Griffith University
[4]Lancaster University
[5]University of Zurich
[6]VU University

November 28, 2022

Abstract

Predicting catchment stormflow responses after tropical deforestation remains difficult. We used five-minute rainfall and storm runoff data for 30 events to calibrate the Green–Ampt (GA) and the Spatially Variable Infiltration (SVI) model and predict runoff responses for a small, degraded grassland catchment on Leyte Island (the Philippines), where infiltration-excess overland flow is considered the dominant storm runoff generating process. SVI replicated individual stormflow hydrographs better than GA, particularly for events with a small runoff response or multiple peaks. Calibrated parameter values of the SVI model (i.e., spatially averaged maximum infiltration capacity, Im and initial abstraction, F0) varied markedly between events, but exhibited significant negative linear correlations with (mid-slope) soil water content at 10 cm (SWC10) – as did the 'catchment effective' hydraulic conductivity (Ke) of the GA model. SWC10-based values of F0 and Im in SVI resulted in satisfactory to good predictions (NSE $>$ 0.50) for 18 out of 26 storms for which data on SWC10 were available, but failed to reproduce the hydrographs for six events (23%) with mostly small runoff responses. Median values of field-measured near-surface Ksat (~2–3 mm h-1, depending on method) were distinctly lower than the median Im (32 mm h-1) and, to a lesser extent, Ke (~8 mm h-1), confirming previously suspected under-estimation of field-measured Ksat. Using pre-storm topsoil moisture content and 5-min rainfall intensities as the driving variables to model infiltration with SVI gave more realistic results than the classic GA approach or the comparison of rainfall intensities with field-measured Ksat.

Stormflow response and 'effective' hydraulic conductivity of a degraded tropical *Imperata* grassland catchment as evaluated with two infiltration models

Zhuo Cheng[1,2], Jun Zhang[3,4,*], Bofu Yu[2], Nick A. Chappell[5],
H.J. (Ilja) van Meerveld[6], and L. Adrian Bruijnzeel[3,7]

[1]*Department of Geography, Beijing Normal University, Beijing, P. R. China*

[2]*Australian Rivers Institute and School of Engineering and Built Environment, Griffith University, Brisbane, Australia*

[3]*Institute of International Rivers and Eco-Security, Yunnan University, Kunming, P. R. China*

[4]*Environmental Modelling, Sensing & Analysis, TNO, Petten, The Netherlands*

[5]*Lancaster Environment Centre, University of Lancaster, Lancaster, United Kingdom*

[6]*Department of Geography, Hydrology and Climate, University of Zurich, Zurich, Switzerland*

[7]*Department of Geography, King's College London, London, United Kingdom*

Corresponding author: Jun Zhang (jzg290@outlook.com)

Key points:

- The Spatially Variable Infiltration model outperformed the Green–Ampt model when simulating hydrographs, especially for multi-peak events.
- SVI-model parameter values varied markedly, but were correlated with antecedent topsoil moisture content
- Model-derived infiltration capacities were much higher than field-measured K_{sat}, regardless of the model or field method used

Abstract

Predicting catchment stormflow responses after tropical deforestation remains difficult. We used five-minute rainfall and storm runoff data for 30 events to calibrate the Green–Ampt (GA) and the Spatially Variable Infiltration (SVI) model and predict runoff responses for a small, degraded grassland catchment on Leyte Island (the Philippines), where infiltration-excess overland flow is considered the dominant storm runoff generating process. SVI replicated individual stormflow hydrographs better than GA, particularly for events with a small runoff response or multiple peaks. Calibrated parameter values of the SVI model (*i.e.*, spatially averaged maximum infiltration capacity, I_m and initial abstraction, F_0) varied markedly between events, but exhibited significant negative linear correlations with (mid-slope) soil water content at 10 cm (SWC_{10}) – as did the 'catchment effective' hydraulic conductivity (K_e) of the GA model. SWC_{10}-based values of F_0 and I_m in SVI resulted in satisfactory to good predictions (NSE > 0.50) for 18 out of 26 storms for which data on SWC_{10} were available, but failed to reproduce the hydrographs for six events (23%) with mostly small runoff responses. Median values of field-measured near-surface K_{sat} (~2–3 mm h^{-1}, depending on method) were distinctly lower than the median I_m (32 mm h^{-1}) and, to a lesser extent, K_e (~8 mm h^{-1}), confirming previously suspected under-estimation of field-measured K_{sat}. Using pre-storm topsoil moisture content and 5-min rainfall intensities as the driving variables to model infiltration with SVI gave more realistic results than the classic GA approach or the comparison of rainfall intensities with field-measured K_{sat}.

Plain Language Summary

It is important for flood management to be able to predict the volume and peak value of streamflow during intense rainfall (so-called 'stormflow'). We used rainfall and streamflow data for a small, degraded tropical grassland catchment on Leyte Island (the Philippines) to calibrate two rainfall infiltration models of different complexity: the simple Green–Ampt model (GA) and the Spatially Variable Infiltration (SVI) model that describes rainfall infiltration into the soil as a function of the intensity of the rain. SVI generally performed better than GA in simulating observed stormflow responses, especially for events with multiple rainfall peaks. Values for the two main parameters of SVI (the amount of rainfall required to initiate stormflow, and the maximum infiltration capacity of the soil) varied with the amount of moisture in the top 10 cm of the soil prior to the rain. Using the measured topsoil moisture contents for 26 rainfall events to estimate the SVI parameter values and predict the stormflow response from the measured rainfall intensity produced satisfactory to good results for ~70% of the examined storms. However, it failed to reproduce the stormflow patterns for six events with mostly small to very small runoff responses.

1 Introduction

Large areas in the humid and seasonal tropics suffer moderate to severe soil degradation (Bai et al., 2008; Gibbs & Salmon, 2015). Repeated cycles of slash-and-burn cultivation, as well as more intensive forms of agricultural cropping and grazing, have resulted in reductions in topsoil organic matter content, soil faunal activity and macroporosity, and an increase in bulk density (Martinez & Zinck, 2004; Shougrakpam et al., 2010; Recha et al., 2012; Zwartendijk et al., 2017; Toohey et al., 2018). The associated decline in soil infiltration capacity typically leads to increased occurrence and amounts of infiltration-excess overland flow (IOF) in regions and/or periods with high rainfall intensities (Chandler & Walter, 1998; Ziegler et al., 2004; Molina et al., 2007; Ghimire et al., 2013; Bush et al., 2020). IOF, in turn, causes accelerated erosion, as well as higher runoff peaks at the headwater catchment scale (Ziegler et al., 2009; Liu et al., 2011; Recha et al., 2012; Ribolzi et al., 2017; Birch et al., 2021a, 2021b), which exacerbates flooding and sedimentation problems downstream (Bruijnzeel, 2004; Sidle et al., 2006; Valentin et al., 2008; Yin et al., 2019).

Despite the extent of tropical land degradation and associated environmental problems, comparatively little progress has been made with the quantitative prediction of storm runoff for degraded tropical catchments (Yu, 2005; Sidle et al., 2006; Ribolzi et al., 2017; Yamamoto et al., 2021; Birch et al., 2021a). Some of the more frequently used approaches include the Green–Ampt infiltration model (GA; Mein & Larsen, 1973; Chu, 1978) and the US Soil Conservation Service curve number (SCS–CN) method (Ponce & Hawkins, 1996). GA partitions rainfall between infiltration and IOF. The SCS–CN method estimates ‘direct runoff’ (*i.e.*, a fast runoff component that is assumed to be linearly related to rainfall) from hillside plots or small catchments using a dimensionless ‘curve number’ (CN-value) that is assumed to capture catchment-wide water retention as a function of soil texture, drainage conditions and land cover/use (Ponce & Hawkins, 1996). Both approaches have their limitations. Although GA takes short-term changes in infiltration rate as the soil wets up during rainfall into account (Koorevaar et al., 1983), the method applies only to individual points. The notoriously high spatial variability of near-surface saturated soil hydraulic conductivity (K_{sat}) makes it difficult to obtain 'representative' estimates at the hillslope- to catchment scale (Sharma et al., 1987; Dunne et al., 1991; Chappell et al., 1998; Zehe & Flühler, 2001; Campos Pinto et al., 2018). Hence, a spatially uniform 'effective' final infiltration rate (K_e) is usually assumed in catchment-scale applications of GA (Aston & Dunin, 1979; James et al., 1992; Nearing et al., 1996; Leemhuis et al., 2007; Yira et al., 2016). More importantly, once infiltration reaches steady-state condition, infiltration rates as predicted by GA do not respond to changes in rainfall input anymore (Yu, 1999), despite ample evidence to the contrary (Hawkins, 1982; Dubrueil, 1985; Dunne et al., 1991; Yu et al., 1997a; Stone et al., 2008). On the other hand, the SCS–CN method is incapable of providing information on the spatio-temporal variation in storm runoff (Garen & Moore, 2005; Ogden et al., 2017). Nevertheless, GA or SCS–CN constitute a core element of widely used erosion and hydrological models, such as WEPP (Flanagan et al., 2001; Nearing et al., 1996) and SWAT (Neitsch et al., 2011; Arnold et al., 2012). Therefore, Ogden et al. (2017) called for the identification of '*more appropriate dynamic hydrological formulations for different hydro-geographic regions*' (such as the tropics) to replace the static and spatially lumped SCS–CN method, as did Yu (1999) in relation to GA (*cf.* Yamamoto et al., 2020).

Arguably, in areas with significant surface degradation, where IOF is likely to be the dominant storm runoff generation mechanism (Sutherland & Bryan, 1990; Mathys et al., 1996; Chandler & Walter, 1998; Molina et al., 2007), a dynamic model of infiltration that takes the spatial variability of surface K_{sat} into account, *as well as* the positive impact of rainfall intensity on infiltration rates (Hawkins, 1982; Dunne et al., 1991), would go some way towards the improved process description called for by Ogden et al. (2017). Building upon earlier work by Hawkins and Cundy (1987), Yu et al. (1997a) developed a spatially variable infiltration model (SVI) that relates actual infiltration rates at the plot scale (as determined by subtracting measured IOF from rainfall over short consecutive periods) to rainfall intensity and a spatially averaged infiltration parameter. SVI proved to be consistently superior to GA with regard to predicting IOF from (mostly large) storms on (mostly bare) hillside plots at various tropical sites (Yu, 1999). Fentie et al. (2002) considered SVI the best choice amongst eight different methods to predict IOF from grazed plots in Queensland, whereas Van Dijk and Bruijnzeel (2004) concluded that SVI provided a '*robust and accurate method for predicting runoff*' from terraced fields on volcanic substrate in Indonesia. Recently, Z. Cheng et al. (2018) compared the performance of GA and SVI under much drier conditions on the Chinese Loess Plateau, and concluded that the amount of simulated IOF was less sensitive to changes in model parameter values for SVI than for GA. Despite SVI's superior performance at the plot scale in a range of tropical settings (Yu, 1999; Fentie et al., 2002; Van Dijk & Bruijnzeel, 2004; *cf.* Patin et al., 2012), the model has so far not been used to predict stormflow at the *catchment scale*. Conversely, GA has been used extensively for this purpose (*e.g.*, Aston & Dunin, 1979; Van Mullem, 1991; James et al., 1992; Obiero, 1996; Conolly et al., 1997; Leemhuis et al., 2007; Yira et al., 2016; Yamamoto et al., 2020).

This paper marks the first attempt to evaluate SVI's ability to predict stormflow hydrographs and peak discharge, using detailed rainfall and streamflow data for the 3.2 ha Basper catchment on Leyte Island (the Philippines). After decades of slash-and-burn, much of the catchment is covered by *Imperata* and *Saccharum* grasses. Fire-climax grasslands constitute a widespread form of degraded land, occupying an estimated area of up to 57 million ha across South and Southeast Asia in the early 1990s (Garrity et al., 1997). More than two-thirds of the estimated 6.5 million ha under *Imperata* in the Philippines (17% of the national land base) were classified as experiencing moderate to severe surface erosion (Concepcion & Samar, 1995). Despite its widespread existence, quantitative hydrological information for this type of grassland is scant (Jasmin, 1976; Lim Suan, 1995; *cf.* Sirimarco et al., 2018). Earlier work in the Basper catchment revealed very low (near-) surface values of K_{sat}, suggesting the likelihood of frequent IOF occurrence, even though K_{sat} may have been under-estimated (Zhang et al., 2019a). Nearly two-thirds of the annual streamflow at

Basper consists of stormflow (here defined as the component of the hydrograph above the Hewlett and Hibbert (1967) separation line), rendering the catchment one of the hydrologically most responsive humid tropical sites described to date (Zhang et al., 2018a; *cf.* Chappell et al., 2012; Birkel et al., 2021). Although no explicit measurements of hillslope IOF were made at Basper, the extreme dilution of streamflow during rainfall events (Zhang et al., 2018a; Van Meerveld et al., 2019) and isotope hydrography separation results (Van Meerveld et al., 2019) all suggest a major contribution of low electrical conductivity 'new water' to stormflow. Hence, our objectives were to: (*i*) test the appropriateness and relative performance of GA and SVI for describing storm runoff for a small catchment in a state of advanced surface degradation; (*ii*) examine the temporal variability of the calibrated model parameters, and their relationships with antecedent soil water content and rainfall characteristics; and (*iii*) compare calibrated model infiltration parameter values with the previous field measurements of K_{sat} by Zhang et al. (2019a) to assess the degree of possible under-estimation of the latter at the catchment scale.

2 Materials and methods

2.1 Study area

The south-facing 3.2-ha Basper catchment (11°15'28" N; 124°57'22" E) is located 14 km west of Tacloban, the capital of Leyte Island. Elevations range from 50–135 m a.s.l. The climate is tropical ever-wet (Köppen-type Af) with a mean annual rainfall at Tacloban Airport (1977–2012) of 2,660 mm (range: 1,435–4,790 mm), distributed over 195 rain days (with ⩾0.5 mm of rain each) on average per year. There is no clear dry season, but average monthly rainfall totals are distinctly higher (>350 mm mo^{-1}) between November and January than for April–May (>100 mm mo^{-1}). Typhoons and tropical storms can bring large amounts of rain and supply roughly one-third of the annual rainfall in the region (Cinco et al., 2016). Between 1977 and 2011, ~50% of all rain days at Tacloban Airport received less than 5 mm of rain. Considering only events with ⩾5 mm of rain, 64% of storms were 5–20 mm in size, whereas 10% and 2.5% of events were larger than 50 and 100 mm, respectively. The median 5-, 15-, 30-, and 60-min rainfall intensities measured at Basper during 99 events with at least 5 mm of rain between June 2013 and May 2014 were 3.2, 2.1, 1.5 and 1.0 mm h^{-1}, respectively. Corresponding 95th-percentile intensities were 34, 22, 18, and 12 mm h^{-1}.

The upper slopes are straight to slightly concave, while foot-slopes generally steepen towards the stream. Landslides are a prominent feature and made up 3.4% of the catchment area at the time of the investigation (Zhang et al., 2018a; Figure 1). The vegetation consists of *cogon* grass (*Imperata cylindrica*) on the ridges and upper slopes, with additional sedge (*Cyperus* sp.) in less well-drained parts. The mid-slope parts have a mixture of *Saccharum spontaneum* grass and low shrub (<1.5 m, mostly *Melastoma* and *Chromolaena*), while shrubs and young trees (<3 m, mostly *Neonauclea* and *Leukosyke*) are common on the lower slopes. Although regularly burned in the past, the area did not experience fire after 2003 and young regenerating forest occupied an estimated 4,500 m^2 (~14%) in the central portion of the catchment at the time of the study (Figure 1).

Eutric Cambisols of predominantly clay loam texture, grading to a sandy clay loam below 90 cm depth, overlay the gabbro bedrock. Soil organic carbon content, porosity and drainable pore space decline with depth, while median bulk densities increase with depth in the top 40 cm (Zhang et al., 2019a). The median (± median absolute deviation, MAD) steady-state surface infiltration rate (determined using a portable double-ring infiltrometer with inner and outer ring diameters of 15 and 21 cm) was 2.1 ± 0.7 mm h^{-1} (n = 13). The median near-surface K_{sat} (<10 cm depth) obtained from small cores (laboratory permeameter) was 1.7 ± 1.6 mm h^{-1} (n = 27). The median K_{sat} at ~20 cm depth as derived with a constant-head well permeameter was 2.7 ± 2.2 mm h^{-1} (Amoozegar, 1989; n = 20; see Zhang et al. (2019a) for details).

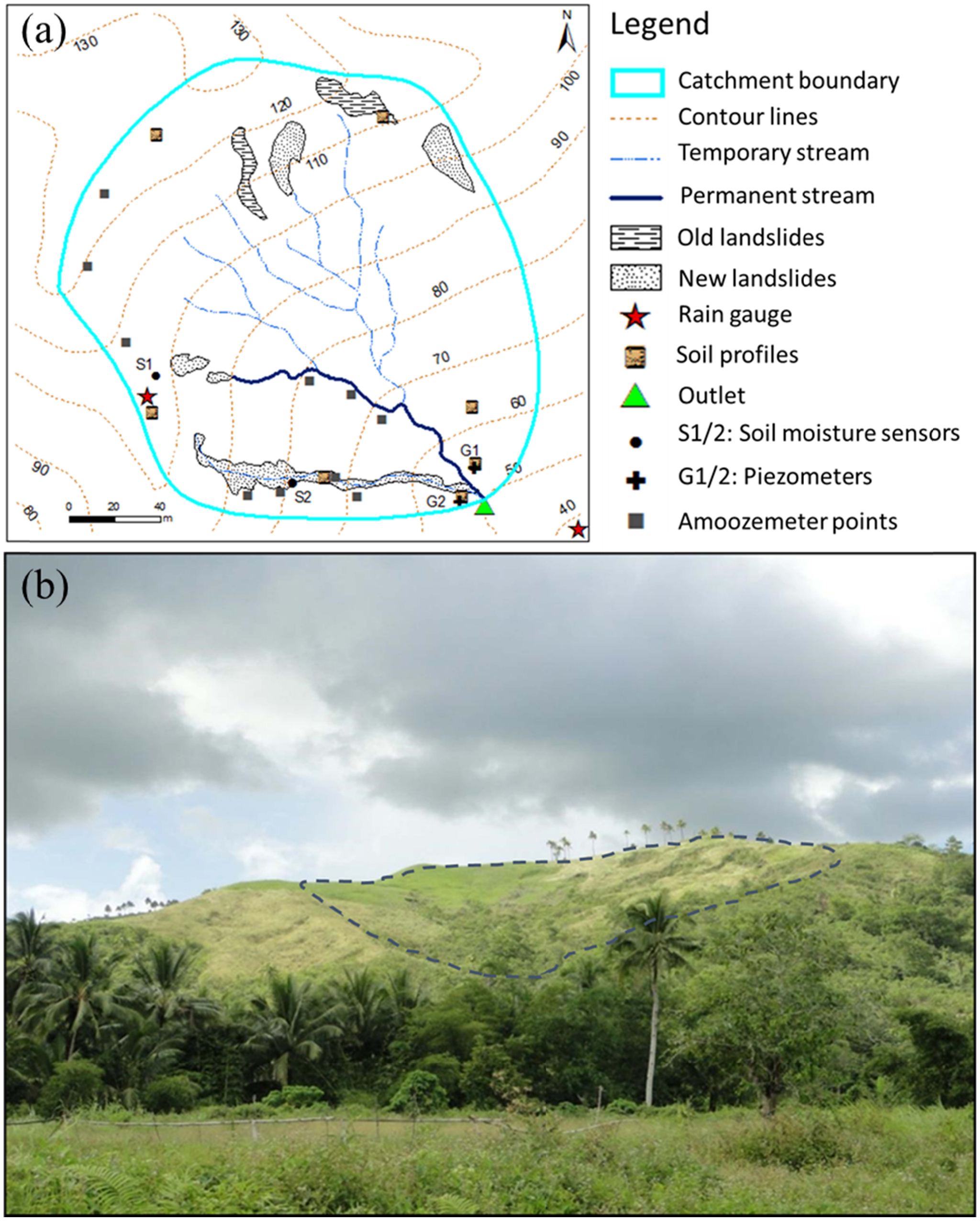

Figure 1. Basper micro-catchment. **(a)** Map showing the drainage network, and locations of landslides, hydrological instrumentation, soil profiles (core sampling and double-ring infiltration sites), and soil hydraulic conductivity measurements using well permeametry. **(b)** Photo showing the land cover. The broken line indicates the catchment boundary. Photo credit: Jun Zhang.

2.2 Methods

2.2.1 Hydrological monitoring

For this study, we used measurements of rainfall, streamflow, soil water content and foot-slope groundwater levels taken between 3 June and 7 November 2013. These measurements represent the conditions prior to the major disturbance to vegetation and soils by Typhoon Haiyan on 8 November 2013 (Zhang et al., 2018a).

Rainfall (P) was measured using two Onset Computer Corporation RG3 tipping-bucket rain gauges (0.25 mm per tip, confirmed by manual calibration) connected to a HOBO Pendant event data-logger. One gauge was located in the open near the catchment outlet and the other on the upper western ridge (Figure 1a). A standard manual rain gauge (100 cm^2 orifice) was placed next to each of the recording gauges and read every morning as a check.

Streamflow (Q) was measured using a sharp-crested compound weir consisting of a 0.55 m high 90° V-notch and a horizontal beam extending 0.5 m to each side from the edge of the V-notch (Zhang et al., 2018a). Water pressure was measured at five-minute intervals using a HOBO U20L04 logger and corrected for atmospheric pressure, which was measured by a similar device in a hut located ~100 m from the weir. The standard V-notch weir equation (Bos, 1989) was checked through volumetric discharge measurements below 4.4 $l\ s^{-1}$ (staff heights < 0.3 m), and Price Type-AA current-meter measurements at stages up to 0.55 m. Water levels exceeded the shoulder of the V-notch for ~1.3% of the total duration of the 30 selected storm events (Section 2.2.2), representing ~33% of the corresponding total storm runoff amount. For these conditions the Bergmann compound weir equation as given by USBR (1997) was used to calculate the streamflow.

Volumetric soil moisture content (θ) *and shallow groundwater levels* were monitored at different sites within the catchment (Figure 1a; Zhang et al., 2018a). The present analysis only used soil moisture data from site S2 (*Saccharum* grassland at mid-slope position) and shallow groundwater levels as measured at piezometer site G1 (left bank, 0.9 m deep; Figure 1a). Soil moisture at S2 was measured at five-minute intervals using simplified Time Domain Reflectometry (TDR) sensors (MP-306, ICT

International, Australia) installed at 0.1, 0.2, 0.4, 0.6, 0.8, and 1.1 m below the surface, and connected to an ICT International Microvolt data-logger. Water levels in piezometer G1 were also measured at five-minute intervals using a HOBO U20L04 logger.

2.2.2 Stormflow separation and event selection

To separate stormflow (Q_q) from baseflow (Q_b), the constant-slope method of Hewlett and Hibbert (1967) was applied to the streamflow record for each event prior to Typhoon Haiyan (3 June–7 November 2013). The following criteria were used to define the start of each ‘stormflow event': (*i*) total rainfall ⩾ 5 mm; and (*ii*) the event was preceded by a rain-free period ⩾ 6 h. For the end of an event, a threshold value of 0.005 mm per five minutes (0.06 mm h^{-1} equivalent) was used. Furthermore, we only included events for which the five-minute rainfall- and streamflow measurements were complete (*i.e.*, no data gaps). Lastly, events for which > 10% of the stormflow could have been generated by precipitation falling directly onto the perennial stretch of the stream (~90 m^2 or 0.28% of the total catchment area; Figure 1a) were excluded. Thus, only events with a minimum hillslope runoff contribution > 90% were considered. Application of the above criteria yielded 30 stormflow events for comparative testing of the Spatially Variable and Green–Ampt infiltration models.

2.2.3 Likelihood of an overland flow dominated system as inferred from the transit time of the rainfall-to-streamflow wave propagation

The extremely low sub-soil K_{sat}-values determined in the field (Zhang et al., 2019a), the high electric conductivity of foot-slope groundwater and pipe flow (~270 μS cm^{-1}) but strong dilution of streamflow during times of stormflow (Zhang et al., 2018a; Van Meerveld et al., 2019), and high event-water contributions to stormflow (Van Meerveld et al., 2019) all suggest that runoff generation in the Basper catchment is dominated by IOF. But before comparing the performance of the GA and SVI models for the prediction of catchment-wide overland flow generation, we investigated whether the selected storm runoff events were more likely to be generated primarily by IOF than return flow and saturation overland flow (SOF) (*cf*. Dunne & Black, 1970; Lapides et al., 2022) in more detail. Using a data-based mechanistic modeling approach, the rainfall-generated streamflow response time was compared to that of the groundwater level in piezometer G1 in the riparian zone that is influenced by lateral subsurface flow. To facilitate the comparison, the observed piezometer water levels were converted to pore-water depth equivalents by multiplying the water levels times the measured soil porosity (Zhang et al., 2019a). The response times (strictly speaking, of the celerities, not of the velocities of the water particles), were identified from optimal Transfer Function (TF) models using the Nash-Sutcliffe model efficiency (NSE; Nash & Sutcliffe, 1970) and a heuristic measure that helps avoid selection of over-parameterised models (the Young Information Criterion; Young, 2001) as selection criteria. A discrete-time, rather than continuous-time, transfer function identification algorithm was used (Chappell et al., 1999) to account for the presence of occasional short breaks in the observed streamflow record. This algorithm, RIVID, is part of the CAPTAIN Toolbox for Matlab (Taylor et al., 2007). A wide range of model structures were evaluated covering first- to third-order models, with pure time delays ranging from zero to 30x the five-minute time-steps, and various non-linearity transformations, including the established Store–Surrogate (Chappell et al., 1999) and Bedford–Ouse approaches (Chappell et al., 2006).

The modeling identified time constants of first-order (*i.e.*, single pathway) models of the rainfall-streamflow response that varied between 9–15 min, depending on the event. These times are much smaller (*i.e.*, the response is much faster) than for the cyclone-affected South Creek basin in Queensland, where hillside SOF is important (Chappell et al., 2012), but comparable to those derived for overland flow plots (*e.g.*, Chappell et al., 2006). This suggests a dominance of IOF at Basper. Further, the subsurface response to rainfall in the riparian zone at Basper (*i.e.*, foot-slope groundwater levels) was 9–70 h and thus much slower than the streamflow response to rainfall (9–15 min), again pointing to IOF as the main mechanism for stormflow generation (see examples in Supporting Information S1).

2.2.4 Infiltration models

Two models of contrasting complexity were used to quantify the infiltration process and to derive the associated amounts of excess rainfall (r_e). However, an identical runoff routing algorithm was employed in both cases for subsequent comparison with the observed storm runoff hydrographs at the catchment outlet.

The first model is based on the Green–Ampt (GA) equation, in which the infiltration capacity (i_c) is expressed as a function of the cumulative infiltration amount, F (in mm) as:

$$i_c = K_e \left(1 + \frac{\psi_m}{F}\right) \tag{1}$$

where K_e (mm h^{-1}) can be regarded as the 'effective' saturated hydraulic conductivity of the surface soil, and ψ_m (mm) as the 'effective' matric potential at the wetting front across the catchment. An application of the GA equation for a rainfall event of constant intensity was developed by Mein and Larsen (1973) and for an event of varying intensity by Chu (1978). Computational procedures are described in detail by Chow et al. (1988). Briefly, for each time interval j, given a rainfall intensity p, and a cumulative infiltration F at the beginning of the interval, there are three possible scenarios for the actual rate of excess rainfall (r_e): (*i*) $p < i_c$, and $r_e = 0$ throughout the interval; (*ii*) ponding condition, *i.e.* $i_c = p$, is met at some point during the time interval; or (*iii*) ponding has occurred and p exceeds i_c throughout the interval, hence $r_e = p - i_c$. In each of the three cases, F is updated to the end of the time interval.

The second model was SVI (Yu et al., 1997a), which conceptualizes overland flow generation during two distinct phases. At the start of an event, i_c is typically much larger than p, and an initial abstraction, F_0 (in mm) is used to represent the amount of infiltration prior to the commencement of excess rainfall. In other words, r_e is zero at this stage – irrespective of rainfall intensity, as long as cumulative rainfall is less than F_0:

$$r_j = 0, when \sum_{i=1}^{j} p_i \leq F_0 \tag{2}$$

Once cumulative rainfall has exceeded F_0, the actual rate of infiltration, i_a is modeled as a function of the rainfall intensity and a spatially averaged maximum infiltration rate, I_m (both in mm h^{-1}). The main assumption behind the SVI model is that i_c varies in space according to an exponential distribution that involves I_m as a single parameter (Yu et al., 1997a; *cf.* Hawkins & Cundy, 1987; Supplementary Figure S1).

It can be shown (Yu et al., 1997a) that:

$$i_a = I_m(1 - e^{-p/I_m}) \tag{3}$$

Application of either SVI or GA leads to a time series of excess rainfall on hillslopes as the difference between rainfall intensity and the modeled rate of infiltration:

$$r_e = p - i_a \tag{4}$$

To take the rain falling directly on the surface of the perennial stream (*i.e.*, channel precipitation; see Section 2.2.2 above for rationale) into account, the total excess rainfall, r^* was expressed as the area-weighted sum of rainfall excess over the stream channel and that over the hillslopes:

$$r^* = (1 - f_w)r_e + f_w p \tag{5}$$

where f_w is the fractional area of the perennial stream channel (in this case: 0.28%).

Regardless of the infiltration model used, for each time interval, j, with excess rainfall computed using equations (4) and (5), r^* is routed to the catchment outlet using a simple kinematic wave approximation:

$$Q_j = \alpha Q_{j-1} + (1 - \alpha) r_j \tag{6}$$

where Q_j is the stormflow rate at the catchment outlet for time interval j (in mm h^{-1}). The routing parameter, α, is related to the catchment lag time, T (in hours), and the adopted time interval for the rainfall and storm runoff observations, Δt as follows (Yu et al., 1997a):

$$\alpha = \begin{cases} T/(T + \Delta t) & T \leq \Delta t/2 \\ (2T - \Delta t)/(2T + \Delta t) & T > \Delta t/2 \end{cases} \tag{7}$$

The advantage of using Equation (6) for routing is the guaranteed numerical stability, irrespective of the magnitude of T relative to Δt.

2.2.5 Model calibration and evaluation

The parameters for the two models were optimized by minimizing the sum of squared errors (SSE) between the observed and modeled stormflow using the Levenberg-Marquardt algorithm (Marquardt, 1963):

$$\min SSE = \sum_{j=1}^{N} \left(Q_j - \hat{Q}_j\right)^2 \tag{8}$$

where $\hat{Q}_j$ and Q_j are the modeled and observed stormflow rates, respectively (in mm h^{-1}), and N is the total number of time intervals for the event. Model parameters were calibrated for each individual event to account for temporally varying infiltration rates, resulting in 30 parameter sets (one for each event) for each of the two infiltration models. The two infiltration models were fully integrated with the Parameter ESTimation Software (PEST++) for efficient parameter estimation (White et al., 2020).

To evaluate model performance, the Nash-Sutcliffe efficiency was calculated for each of the 30 individual storm runoff hydrographs. Further, we computed the Sum of Squared Errors, percent bias (PBIAS; Gupta et al., 1999), and the ratio between the RMSE of the observations and their standard deviation (RSR; Legates & McCabe, 1999) for each event. Although the two infiltration models were applied primarily to test their ability to predict storm hydrographs at five-minute intervals, model performance was also examined in terms of stormflow amount (Q_q) and peak runoff rate (Q_p) for individual events.

2.2.6 Relations between infiltration model parameters and event characteristics

The calibrated infiltration model parameters were related to event rainfall characteristics to examine whether – and to what extent – the model parameters were affected by rainfall characteristics and antecedent conditions. The main event characteristics used in the Spearman rank correlation analysis were the peak intensity and the maximum rainfall intensities during 15 and 30 min. The main indicators of antecedent wetness conditions were the three-day antecedent precipitation index (API_3) and the volumetric water content in the top 10 cm of the soil at mid-slope position (SWC_{10}). The Antecedent Precipitation Index (API) is a measure of catchment wetness based on the rainfall that occurred over preceding days and was calculated as:

$$API = \sum_{n=1}^{N} P_n k^n \tag{9}$$

where P_n is the precipitation during the n^{th} day preceding the day for which the API is calculated, and k is a decay constant. Given the small size and comparatively shallow soils of the study catchment, we decided to use a three-day antecedent precipitation index (API_3) using a k value of 0.80 (Shaw et al., 2010).

2.2.7 Comparison of hydraulic model parameters with field measurements

The point-measured K_{sat} data from Zhang et al. (2019a) were compared directly with the model-calibrated values of near-surface K_{sat} (*i.e.*, K_e in GA and I_m in SVI). In addition, the *distributions* of the two data series were compared, noting that the underlying idea of the SVI model is that the spatial variation in infiltration capacity i_c can be described by an exponential distribution of the maximum infiltration capacity I_m according to Equation (3) (Yu et al., 1997a). To approximate an overall distribution of i_c for the Basper catchment, the 30 event-based values of I_m were each inserted separately into Equation (3) to derive the corresponding distributions of i_c. The average distribution for all 30 events was regarded as representing the overall spatial distribution of i_c across the catchment. Because differences in mean field K_{sat} based on portable-ring infiltrometry (n = 13), near-surface well permeametry (n = 20), and laboratory permeametry on small cores (n = 27) were not statistically significant (p-value > 0.35), all data were bulked (n = 60).

3 Results

3.1 Characteristics of selected storm events

Rainfall amounts for the 30 events ranged from 6.6 to 149 mm, with a mean of 26 mm (median 18.5 mm; Figure 2). Event total stormflow at the catchment outlet varied from 0.3 mm to 76 mm, averaging 7.2 mm (median 3.5 mm), while stormflow runoff coefficients (Q_q/P) ranged from 3–56%, averaging 21% (median 18%). Collectively, these events represented ~66% of the total rainfall during the 3 June–7 November 2013 study period (1,187 mm) and ~92% of the total storm runoff (235 mm; Zhang et al., 2018a). Event duration (defined as the time between the initial rise in discharge and the stormflow cut-off point; Section 2.2.2) varied from 0.8 to 40.8 h, averaging 10.4 h (median 6.0 h). Event-averaged rainfall intensity (4.3 mm h^{-1}; median 3.3 mm h^{-1}) was approximately an order of magnitude smaller than the five-minute peak rainfall intensity (average: 58 mm h^{-1}, median 55 mm h^{-1}; Figure 2). Based on their Q3/Q1-ratios (*i.e.*, between the third and first quantiles), rainfall amounts and peak rainfall intensities varied less between events than stormflow amounts and peak runoff rates (Figure 2).

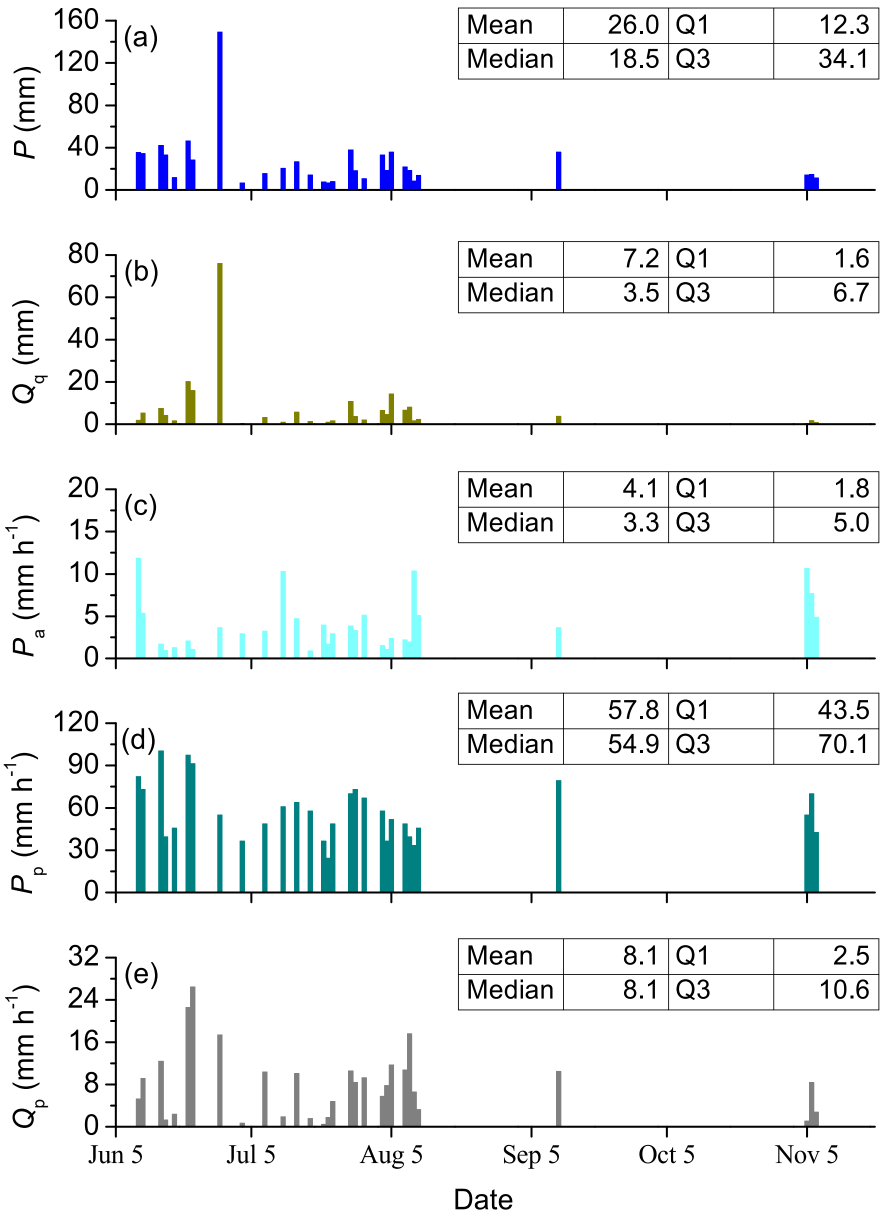

Figure 2. Time series showing the basic characteristics of the 30 examined runoff events at Basper catchment between 6 June and 7 November 2013: **(a)** rainfall (P, mm), **(b)** total stormflow (Q_q, mm), **(c)** average rainfall intensity (P_a, mm h^{-1}), **(d)** peak rainfall intensity (P_p, mm h^{-1}) and **(e)** peak stormflow rate (Q_p, mm h^{-1}). Insets list the means, medians, as well as the first (Q1) and third (Q3) quantiles for the respective variables.

3.2 Comparative infiltration model performance

GA and SVI could be calibrated equally well to simulate event-based Q_q and Q_p, with simulated Q_q and Q_p being in good agreement with observed values (R^2-values of 0.98 and 0.99, respectively, regardless of the model used; Figure 3). Nevertheless, the median Q_q tended to be under-estimated by about 10% (GA) to 14% (SVI; Table 1) and by 21–22% for larger events (based on the slopes of the regression lines in Figure 3a). Peak runoff rates were under-estimated by about 8–12% (Figure 3b; Table 1). However, based on the higher NSE- and lower RSR-values, SVI performed slightly better than GA in terms of simulating event-based stormflow (Table 1).

Table 1. Model performance of SVI and GA for the prediction of storm runoff totals (Q_q) and peak runoff rates (Q_p) for the 30 examined storm events.

Model	Evaluation	Min	Q1	Median	Q3	Max
SVI	SSE[1] (Calibration)	0.04	1.6	4.6	23	418
	NSE[2]	0.57	0.84	0.92	0.95	0.99
	PBIAS[3]_Q_q	-2	6	14	26	54
	PBIAS[3]_Q_p	-12	2.5	8	18	39
	RSR[4]	0.10	0.23	0.28	0.40	0.66
GA	SSE[1] (Calibration)	0.03	2.1	6.8	29.5	589
	NSE[2]	0.12	0.74	0.88	0.94	0.99
	PBIAS[3]_Q_q	-10	-0.8	10	28	60
	PBIAS[3]_Q_p	-6	5	11.5	26	63
	RSR[4]	0.10	0.25	0.35	0.51	0.94

[1]Sum of squared errors; [2]Nash-Sutcliffe efficiency; [3]Per cent bias; [4]Ratio between the RMSE and the standard deviation of the observations

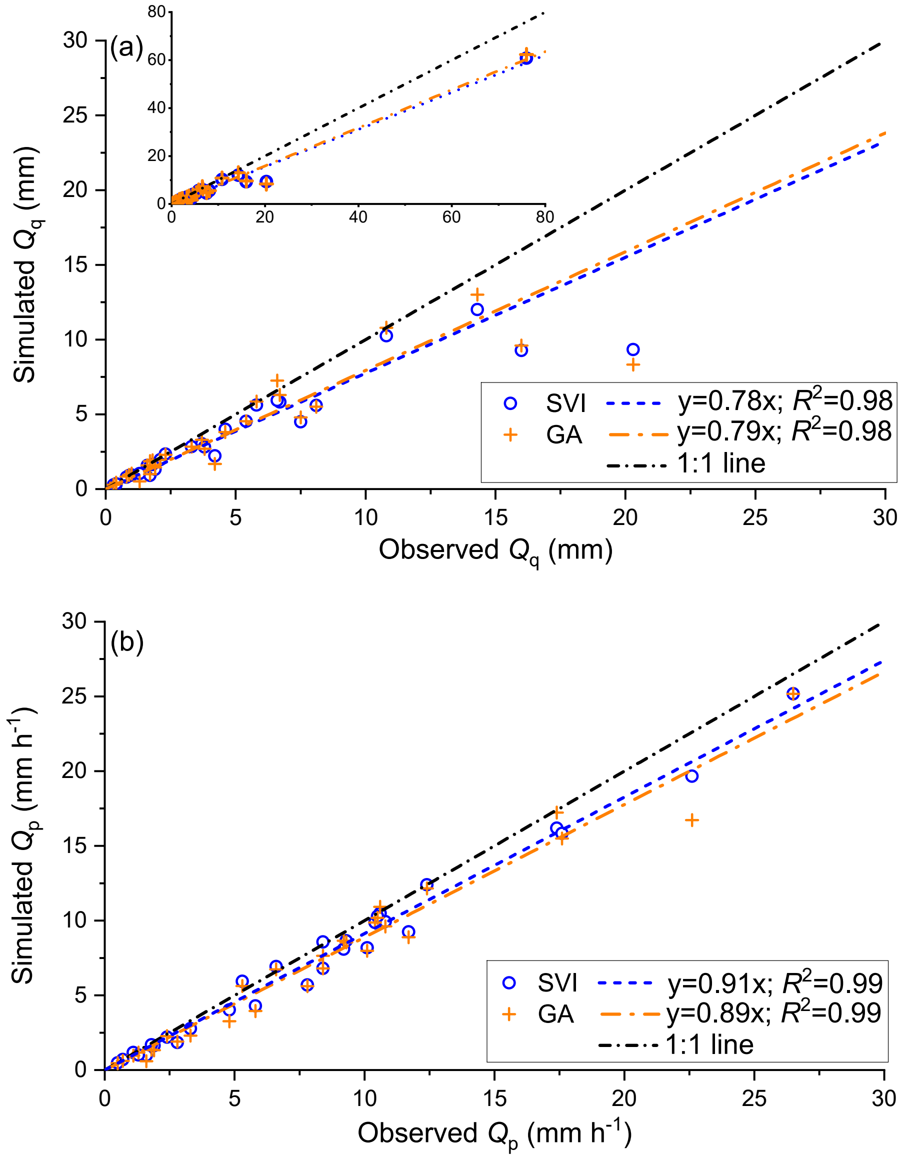

Figure 3. Comparison of the observed and modeled **(a)** stormflow totals (Q_q, mm) and **(b)** peak runoff rates (Q_p, mm h^{-1}) for the 30 examined runoff events. The models were calibrated for each individual event by minimizing the sum of squared errors.

Figure 4 shows the model performance in terms of the NSE-values derived for individual events *versus* corresponding stormflow runoff coefficients ($R_c = Q_q/P$). As indicated by the enveloping line, both models captured events with higher runoff coefficients better than events with lower R_c, for which low NSE-values suggested a poor model fit (Figure 4). Overall, SVI outperformed GA in terms of its ability to reproduce event-based hydrographs, with average NSE-values for all 30 events of 0.88 for SVI *versus* 0.81 for GA (difference significant at a p-value < 0.05). Out of 13 events with $R_c \leq 0.16$, three were captured poorly by GA (*i.e.,* NSE ≤ 0.50) *versus* none for SVI (Figure 4). Simulations for two specific events with multiple runoff peaks are presented in Figure 5 to illustrate the difference in model performance for complex events. GA missed the second peak of the hydrograph entirely for both events, whereas SVI was capable of simulating all peaks despite a certain degree of under-estimation. A similar pattern was noted for the events with a particularly high rainfall intensity at the beginning of the storm, which caused GA-modeled stormflow to occur earlier than observed (see Supplementary Figures S2a and S2b).

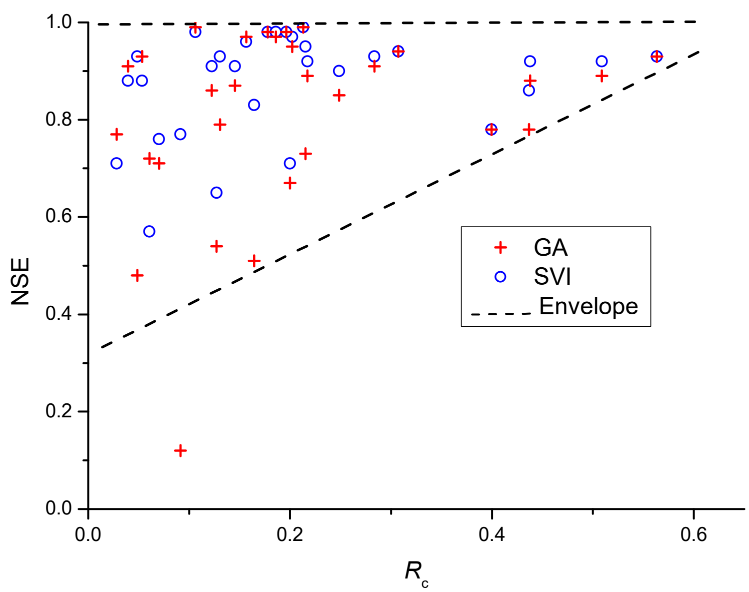

Figure 4. Relationship between stormflow runoff coefficient (R_c) and the Nash–Sutcliffe model efficiency as a measure of model performance for the GA and SVI models for the 30 examined events.

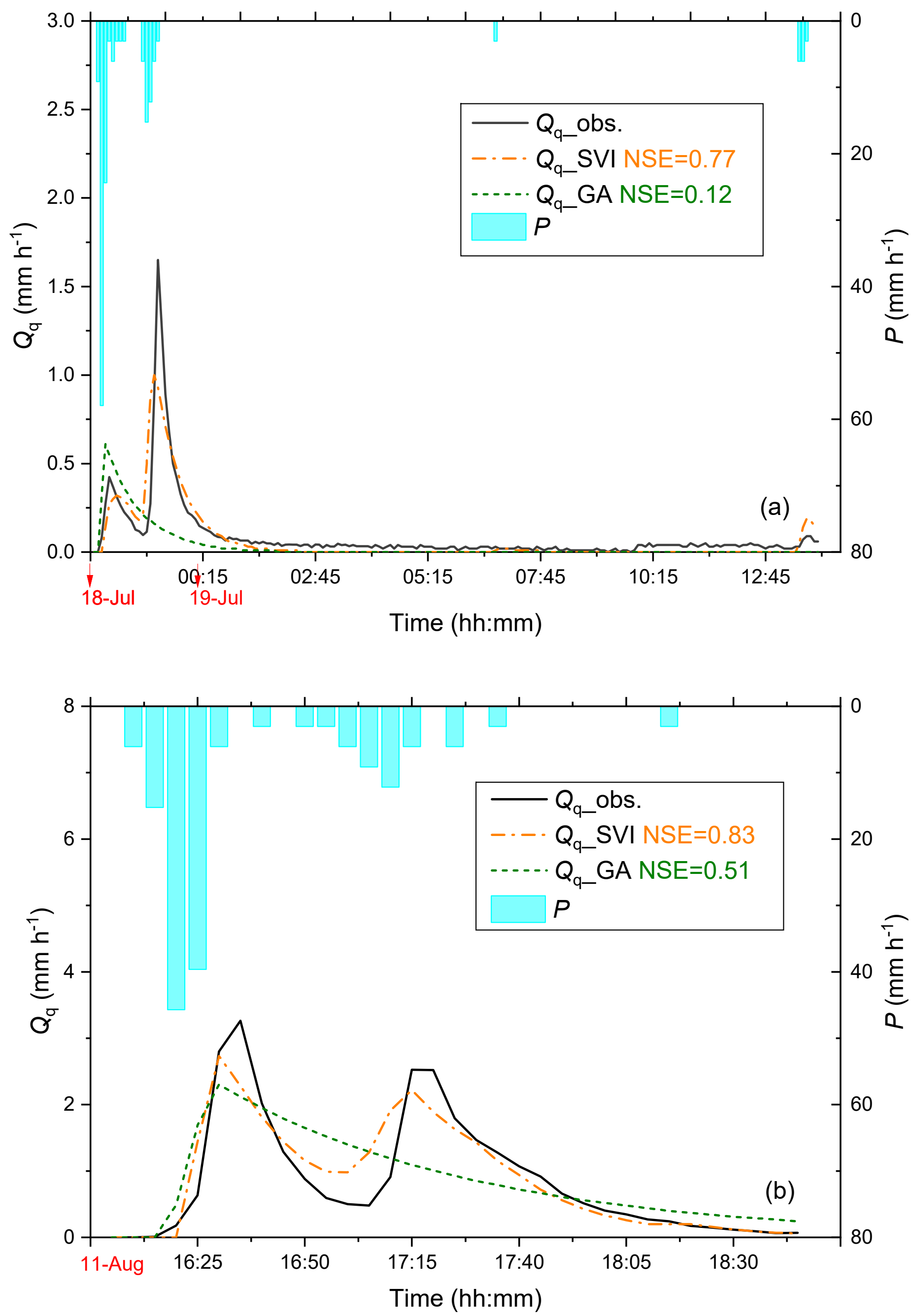

Figure 5. Observed and simulated stormflow hydrographs for two example events with two runoff peaks for which SVI outperformed GA due to the latter's failure to simulate the consecutive peaks: **(a)** the 14 mm event of 18–19 July 2013, with a stormflow runoff coefficient (R_c) of 10%, and **(b)** the 14 mm event of 11 August 2013, with R_c of 17%.

3.3 Infiltration model parameter variability

The optimized values for the three parameters for each infiltration model (F_0 and I_m for SVI; K_e and ψ_m for GA, plus lag time T in both models) are summarized in Table 2. Coefficients of variation (CV) were larger for I_m and K_e compared to the other parameters. The comparison of the ratio of the third and first quantiles (Q3/Q1) suggests that K_e and lag time T in GA varied more from event to event than I_m and T in SVI. Mean lag times for the two infiltration models did not differ significantly (p-value = 0.19).

Table 2. Variability of the optimized infiltration model parameters for the 30 examined events: F_0 = initial abstraction (mm), I_m = spatially averaged maximum infiltration capacity (mm h^{-1}), T = lag time (min), K_e = 'effective' final infiltration rate (mm h^{-1}), and ψ_m = matric potential at the wetting front (mm). Q1, Q2 and Q3 indicate the 1st, 2nd and 3rd quantiles of the respective parameter values. CV denotes the coefficient of variation and C_s the skewness.

Model	Model parameter	Q1	Q2	Q3	Mean	CV	Q3/Q1	C_s
SVI	F_0	5.1	7.0	9.4	7.9	0.5	1.8	1.2
	I_m	22.9	31.6	48.7	47.8	1.1	2.1	2.5
	T	8.6	14.0	19.9	16.9	0.7	2.3	1.7
GA	K_e	3.1	7.5	11.7	9.4	0.9	3.8	1.3
	ψ_m	21.9	24.6	27.4	27.8	0.7	1.2	1.4
	T	12.0	22.3	32.0	25.9	0.6	2.7	0.8

The infiltration-related parameters F_0, I_m and K_e (but not ψ_m) were all positively affected by rainfall intensity (regardless whether represented by the five-minute peak intensity P_p, or maximum intensities over 15 or 30 min, P_{15} or P_{30}), whereas the lag time for either infiltration model was inversely related to rainfall intensity (Table 3). Furthermore, both F_0 and I_m exhibited significant, negative correlations with SWC_{10} (Figure 6), but not with API_3. So did K_e to a lesser extent, but not ψ_m (Table 3).

Table 3. Spearman rank correlation coefficients between the infiltration model parameters and selected rainfall and catchment wetness characteristics: P = event precipitation (mm), P_a= average rainfall intensity (mm h^{-1}), P_p, P_{15} and P_{30} = maximum 5-min, 15-min and 30-min rainfall intensities (mm h^{-1} equivalents), API_3 = three-day antecedent precipitation index (mm), SWC_{10}, SWC_{30} and SWC_{60} = mid-slope soil water contents (%) down to 10 cm, 30 cm, and 60 cm depth, respectively.*** indicates p-value < 0.001, ** p-value < 0.05, * p-value < 0.1.

	P	P_a	P_p	P_{15}	P_{30}	API_3	SWC_{10}	SWC_{30}	SWC_{60}
F_0	0.23	0.34^{*}	0.51^{***}	0.52^{***}	0.46^{**}	-0.13	-0.59^{***}	0.09	0.14
I_m	0.47^{***}	0.22	0.63^{***}	0.63^{***}	0.63^{***}	0.01	-0.57^{***}	0.10	0.21
T_SVI	0.03	-0.34^{*}	-0.38^{**}	-0.48^{***}	-0.35^{*}	-0.27	0.11	-0.17	-0.05
K_e	0.53^{***}	0.06	0.74^{***}	0.72^{***}	0.68^{***}	-0.03	-0.48^{**}	-0.16	-0.20
ψ_m	-0.25	0.288	-0.13	-0.11	-0.14	-0.06	-0.01	0.21	0.33
T_GA	-0.08	-0.23	-0.36^{**}	-0.45^{**}	-0.37^{**}	-0.39^{**}	0.05	-0.37^{*}	-0.30

3.4 Stormflow prediction using SVI

Because the optimized values of the infiltration-related parameters in SVI (*i.e.*, F_0 and I_m) varied considerably between events (Table 2), predictions of individual stormflow hydrographs using average or median parameter values might not be very satisfying (see example events with wet and dry antecedent conditions in Supplementary Figure S3). However, both F_0 and I_m were clearly related to the near-surface wetness condition of the catchment as represented by the moisture content of the top 10 cm of the soil as measured in mid-slope position (though not by that down to 30 or 60 cm, nor by API_3; Table 3). Hence, the linear relationships between SWC_{10} and F_0 or I_m shown in Figure 6 were used to estimate the values of F_0 and I_m for each of the 26 events for which SWC_{10}-data were available. For each event, we used the median value of the lag time (T = 14.0 min).

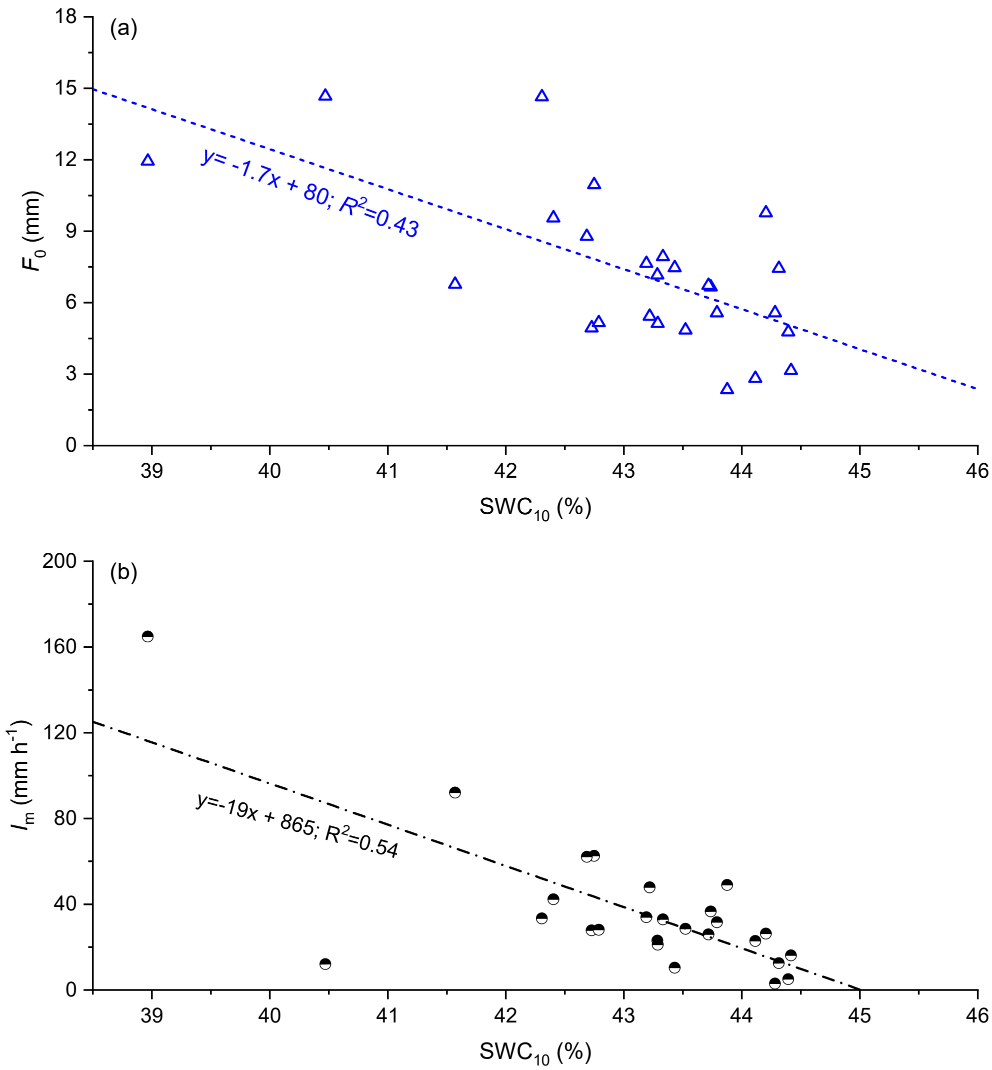

Figure 6. Linear relationships between mid-slope soil water content at 10 cm depth (SWC_{10}) and the optimized parameter values for **(a)** spatially average maximum infiltration rate, I_m, and **(b)** initial abstraction, F_0 for all 26 runoff events for which SWC_{10} data were available.

Satisfactory to good (NSE > 0.5) results were obtained for ~70% of the 26 events with group-based average stormflow runoff coefficients ($R_c = Q_q/P$) larger than ~0.15 (Figure 7). However, SVI was less successful at capturing the stormflow hydrographs of two events with contrasting runoff responses (NSE 0.18–0.28; Figure 7).

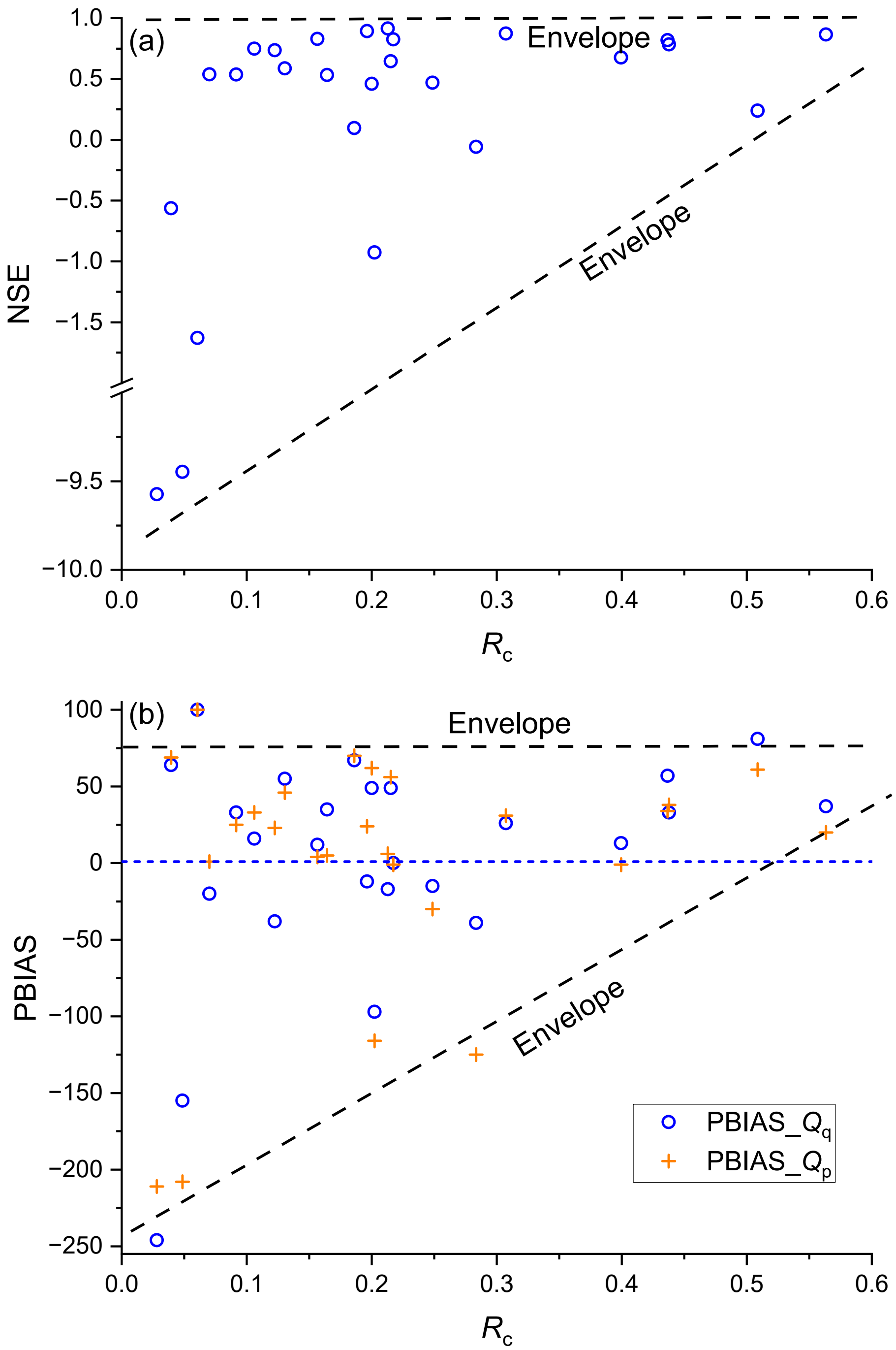

Figure 7. Relationship between stormflow runoff coefficient (R_c) and **(a)** the Nash–Sutcliffe model efficiency (NSE) when the SVI model parameters are based on the correlation with soil moisture at 10 cm ($F_0 = -1.7 \cdot SWC_{10}+80$; $I_m = -19 \cdot SWC_{10}+865$, according to Figure 6); and **(b)** PBIAS for stormflows (PBIAS_Q_q) and peak flow rates ((PBIAS_Q_p).

Negative NSE-values were obtained for another six events (23%) representing mostly (but not exclusively) low stormflow runoff coefficients (Figure 7). Two of these six events had comparatively low rainfall amounts (6.6–7.6 mm) and stormflow totals were severely under-estimated by the model. The remaining four events received more substantial amounts of rain (14–38 mm), but SVI over-estimated the amounts of stormflow considerably. Therefore, a comparison was made between calibrated and estimated values of F_0 and I_m (n = 26) for different classes of NSE and PBIAS; Supplementary Figure S4). Discrepancies between predicted and calibrated values of F_0 had a significant impact on the model performance (*i.e.*, lower NSE), whereas discrepancies in I_m had a smaller effect (Supplementary Figure S4a). Discrepancies in both F_0 and I_m had an important and significant effect on the simulated amount of stormflow (Supplementary Figure S4b). Higher values of F_0 and I_m led to underestimation of stormflow and *vice versa* (Supplementary Figure S4b).

3.5 Comparison of modeled infiltration parameters and measured K_{sat}

The average value for the highly skewed distribution of measured near-surface K_{sat} (22 ± 94 mm h^{-1} *versus* a median of 2 mm h^{-1}; skewness: 6.4) was roughly half the ~42 mm h^{-1} derived from the averaged exponential distribution of infiltration capacities for the 30 events (skewness: 2; Figure 8). In addition, the shape of the two distributions differed in that comparatively low infiltration capacities (< 20 mm h^{-1}) were encountered far more frequently during the field measurements than implied by the modeling, whereas the reverse applied for intermediate (20–50 mm h^{-1}) and higher infiltration capacities (50–500 mm h^{-1}; Figure 8).

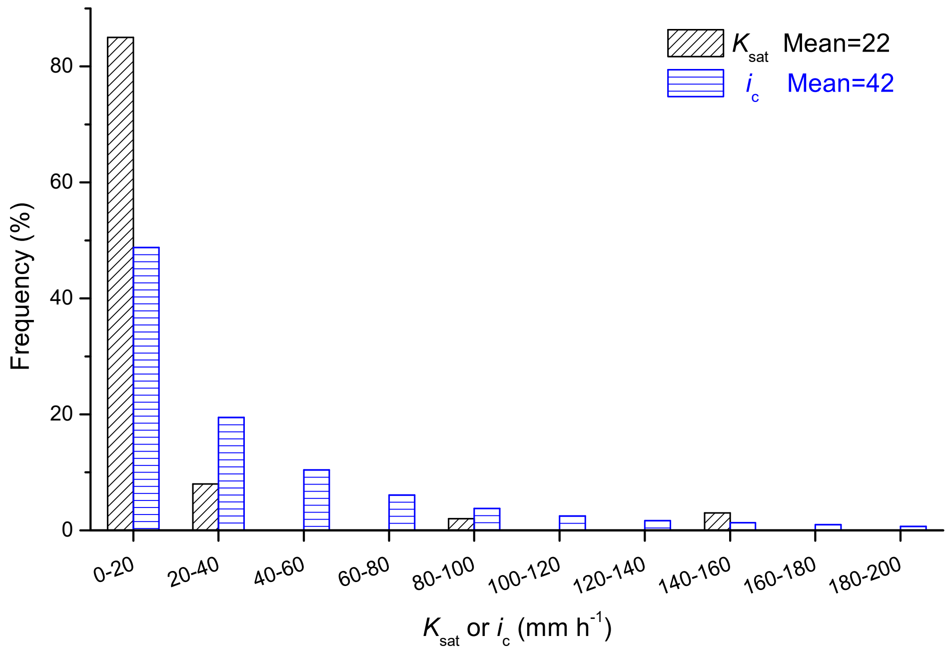

Figure 8. Comparison of the spatial distributions of measured K_{sat} (n = 60; data from Zhang et al., 2019a) and the modeled infiltration capacity (i_c) based on individual values of I_m for all 30 examined events.

4 Discussion

4.1 Infiltration model performance

With median NSE-values of 0.88 and 0.92, respectively, both GA and SVI performed well for the 30 examined events, with a few notable exceptions. In comparison to SVI, GA is inherently not responsive to changes in rainfall intensity, especially after infiltration reaches steady-state conditions (Yu, 1999). This is likely the main reason why GA was not able to reproduce events with consecutive peaks as well as SVI (Figure 5). Further, high-intensity rain falling on an initially dry soil causes the infiltration capacity to decrease rapidly to values approaching an 'effective' K_e (*cf.* Supplementary Figure S1). If subsequent rainfall intensities are less than K_e, this leads to the simulation of low stormflow rates (Figure 5a). Similarly, for events with a particularly high rainfall intensity at the beginning of the storm, the simulation led to large decreases in infiltration capacity within a short period of time, causing GA-modeled stormflow to occur earlier than observed (Supplementary Figure S2). However, SVI did not perform perfectly for events with multiple bursts of rain either. The main reason for this discrepancy lies in the use of constant values for the model parameters for a given event. This assumption is likely to be violated during events with multiple rainfall peaks. An example of this occurred on 3–4 August 2013, when three successive bursts occurred within the event (Supplementary Figure S2c). The first burst occurred on 3 August between 15:20–17:45, the second on 4 August between 00:40–02:45, and the third between 03:20–12:35. The modest runoff peak for the second burst was greatly over-estimated, whereas the larger, third peak was substantially under-estimated (Supplementary Figure S2c). This is likely because the time gap between the first and second bursts (~7 h) was large enough to allow the soil to drain somewhat, thereby re-creating some additional storage opportunity. As a result, part of the rainfall of the second burst was used to fill this additional capacity, causing predicted stormflow rates to be over-estimated. For the third burst, which followed soon after (Supplementary Figure S2c), a lower value of I_m than the applied constant value would have been more appropriate to reflect the wetter soil conditions during this part of the event. Instead, applying a higher, constant I_m throughout the event led to under-estimated stormflow rates for the third burst. A similar under-estimation was also noted for the latter part of the event occurring the following day (Supplementary Figure S2d), where a lower I_m would again have given better results.

Both models performed fairly for several events with low stormflow runoff coefficients, even though they were calibrated for these events (*i.e.,* $Q_q/P < 0.10$; Supporting Figures S2e and S2f; *cf.* Figure 4). When applied in predictive mode with F_0 and I_m estimated from mid-slope SWC_{10} (Figure 6), SVI behaved less than satisfactorily for several other events with (mostly) low runoff coefficients (Figure 7).

4.2 Infiltration model parameters: variability and influences

Calibrated values for initial abstraction loss (F_0) and spatially averaged maximum infiltration capacity (I_m) in SVI, as well as for the 'catchment effective' infiltration capacity (K_e) in GA, varied substantially between the 30 examined events, with overall Q3/Q1-ratios of 1.8, 2.1, and 3.8, respectively (Table 2). As expected on the basis of general infiltration theory (Brutsaert, 2005), all three parameters were negatively correlated with topsoil moisture content (SWC_{10}), albeit not with moisture contents down to greater depths, nor with the three-day antecedent precipitation index (Table 3). Patin et al. (2012) did not find clear relationships between I_m and API per land cover for numerous 1-m^2 microplots under various land covers in Lao PDR either, but low values were derived at the height of the rainy season and maximum values late in the dry season. In addition, temporal variability in I_m of soils under young fallow vegetation after slash-and-burn cropping (as practiced in the past at Basper; Zhang et al., 2019a) was markedly greater than that for bare soil, upland rice or *Imperata* grassland. Patin et al. (2012) concluded that variations in the water use of (taller) vegetation types between rainfall events affected I_m through modification of soil water contents in more subtle ways than could be captured by a proxy like API with a stationary (*i.e.*, fixed) recession constant (*cf.* Eq. (9)) that does not capture variations in wetness conditions due to differences in evapotranspiration rates. As such, linking infiltration model parameter values to measured topsoil moisture contents is to be preferred (*cf.* Figure 6). In line with the findings of Patin et al. (2012), I_m at Basper also varied seasonally. Calibrated values less than 50 mm h^{-1} were obtained for events during the rainy June–August period, increasing to 75–175 mm h^{-1} during the drier September–November period (Supplementary Figure S5).

The presence of a well-developed vegetation cover affects the magnitude of I_m and F_0 also in other, indirect ways. Vegetation provides protection of the soil surface against rain drop impact, slaking and crust formation (Wiersum, 1985; Rose et al., 1997; Durán-Zuazo & Rodríguez-Pleguezelo, 2008; Miyata et al., 2009; Lacombe et al., 2018), and promotes soil faunal activity and macropore formation, thereby enhancing infiltration (Blanchart et al., 2004; Shougrakpam et al., 2010; Zwartendijk et al., 2017; Toohey et al., 2018). Indeed, the strongest correlation between I_m and any particular soil characteristic in the Laotian study by Patin et al. (2012) was that with the extent of surface crusting. Hence, comparative median values of I_m for different land-cover types effectively reflected their capacity to prevent crust formation (low for bare soil, high for fallows). Crusting was not studied explicitly at Basper, but the low infiltration capacities recorded by Zhang et al. (2019a) were attributed primarily to erosion during former slash-and-burn cropping phases that exposed the denser sub-soil to the impact of rain drops, as well as a general absence of soil biotic activity and macropores (Quiñones, 2014), and inherent limitations of the K_{sat} measurements (see also discussion below). Repeated cycles of slash-and-burn agriculture can effectively destroy the macropore systems formed during fallow periods (Shougrakpam et al., 2010; Zwartendijk et al., 2017). Pertinently, soil moisture contents at 60 cm depth in the Basper grassland hardly responded to fluctuations in rainfall (Zhang et al., 2018a). Conversely, soil moisture at the same depth beneath a nearby forest responded rapidly to rainfall (Zhang et al., 2018b), suggesting the presence of preferential flow pathways that allowed rapid percolation to deeper layers (Van Meerveld et al., 2019; Zhang et al., 2019a; *cf.* Y. Cheng et al., 2018).

In line with the trend noted above for I_m, F_0 can also be expected to be higher for well-vegetated or mulched surfaces than for bare soils (Yu et al., 1997b; Van Dijk & Bruijnzeel, 2004). The limited data available for tropical sites do not suggest that soil texture has a notable influence on the magnitude of F_0 or I_m (in contrast to findings for K_e by Nearing et al., 1996). Increases in soil organic matter content (SOM) tend to have a positive effect, whereas increases in bulk density tend to have a negative effect (Coughlan, 1997; Yu et al., 1997b; Van Dijk & Bruijnzeel, 2004). However, with the possible exception of the relationship between I_m and bulk density ($R^2 = 0.923$, $n = 7$), the predictive capacity of such tentative equations is still low (Supplementary Figure S6) and many more empirical data are required.

The currently derived median F_0 (7.6 mm, Table 2) exceeded most of the values reported by Yu et al. (1997b) for various bare agricultural plots in Southeast Asia and Queensland (2.3–6.0 mm), which generally had higher bulk densities and lower SOM than the Basper grass- and shrubland (Coughlan, 1997; Zhang et al., 2019a; Supplementary Figure S6). Higher values of F_0 were obtained at the same sites after application of a surface mulch (~13 mm; Yu et al., 1997b). As such, the interception storage capacity afforded by the tall grasses and shrubs at Basper (and their litter) may well have raised the effective value of F_0 somewhat (*cf.* Leopoldo et al., 1981; Waterloo et al., 1999; Bruijnzeel, 1988). In addition, it cannot be excluded that variations in rainfall intensity at Basper further affected the magnitude of F_0 indirectly through variations in wet canopy evaporation rates between successive storms as observed in a nearby forest by Zhang et al. (2018b). This would not only go some way towards explaining the positive correlations between F_0 and short-term rainfall intensities (P_{15} and P_{30}; Table 3), but possibly also the discrepancies between SWC_{10}-based estimates of F_0 and calibrated values for certain poorly predicted events (negative NSE; Supplementary Figure S4a).

4.3 Difficulty of estimating effective hydraulic conductivity and infiltration capacity from point measurements

The median values of the model-based estimates of catchment-wide 'effective' (K_e) and 'maximum' (I_m) infiltration (7.5 mm h^{-1} for GA and 31.6 mm h^{-1} for SVI) were distinctly higher than the field-based measurements of K_{sat} (1.7–2.7 mm h^{-1}, depending on the method used; Zhang et al., 2019a). Also, the SVI-inferred *distribution* of infiltration capacities suggested generally higher values compared to the results obtained by the measurements (Figure 8). However, the measured values were also much lower than the median value reported for similarly textured, non-grazed *Imperata* grassland soils elsewhere in the Palaeo-tropics (35 mm h^{-1}, n = 8; range: 15–95 mm h^{-1}; Zhang et al., 2019a; Ghimire et al., 2021). The methods used for measuring near-surface K_{sat} at Basper may have under-estimated actual hydraulic conductivities to some extent – either because of under-sampling of macropores in the case of small cores and small-diameter ring infiltrometry (Davis et al., 1996; Lai &

Ren, 2007) or due to smearing of boreholes during augering in the case of well permeametry (Sherlock et al., 2000; Bonell et al., 2010). In addition, it cannot be excluded that somewhat higher values of K_{sat} may have been associated with the denser (less penetrable) parts of the regenerating vegetation in the central part of the catchment, where only a few K_{sat} measurements were conducted (Figure 1a). As such, overall mean catchment-wide K_{sat} may also be higher than inferred from the measurements by Zhang et al. (2019a) due to the spatial bias in field sampling. Furthermore, point-measured K_{sat}-values typically under-estimate the 'block permeabilities' of whole hillslopes (Wen & Gomez-Hernandez, 1996; Chappell et al., 1998; Brooks et al., 2004; Pirastru et al., 2017). This under-estimation of block permeability is also seen where statistical distributions of point-measured K_{sat} values are compared directly with 'effective' parameter values derived from inversion of catchment models (*e.g.*, Beven, 1989; Blöschl & Sivapalan, 1995; Mertens et al., 2005).

Both I_m and K_e are commonly applied to characterize soil infiltration capacity (Yu, 2000; Nearing et al., 1996). The relationship between the two is of interest because it allows derivation of modeled I_m (the spatially averaged *maximum* infiltration capacity) from K_e (the 'effective' infiltration rate after reaching steady-state conditions; *cf.* Supporting Figure S1) obtained by inverse means from either IOF (plots) or stormflow (catchments) measurements and GA (*e.g.*, Nearing et al., 1996). In agreement with these definitions, derived values for I_m at Basper (3–259 mm h^{-1}) were higher than those for K_e (1–31 mm h^{-1}). As also reported by Yu (1999) for six different locations in Australia and Southeast Asia, I_m at Basper was positively correlated with K_e. As shown in Supporting Figure S7, the second-order polynomial describing the relation between K_e and I_m for the Basper grassland had an R^2 of 0.45 (n = 30) compared to R^2 = 0.80 (n = 60) for the equation derived by Yu (1999). Additional empirical data for different tropical locations are desirable to complement these tentative equations.

5 Conclusions

Five-minute rainfall and runoff data collected during 30 events (6.6–149 mm of rain) were used to calibrate two infiltration models of different complexity for the prediction of stormflow responses for a 3.2 ha fire-climax grassland catchment at Basper, Leyte Island (the Philippines). The catchment has soils with very low hydraulic conductivity (K_{sat}) and infiltration-excess overland flow is inferred to be the dominant storm runoff generation mechanism. Landslide scars with low-infiltrability slip surfaces are prominent, covering 3.4% of the area.

In the Green–Ampt model (GA), the infiltration rates decline steadily after the start of infiltration, whereas the Spatially Variable Infiltration model (SVI) describes infiltration as a function of short-term fluctuations in rainfall intensity. SVI systematically reproduced the observed stormflow hydrographs better than GA, especially for events with multiple peaks. Calibrated values of the parameters for SVI (notably, spatially averaged maximum infiltration capacity, I_m and initial abstraction, F_0) varied markedly between events, and showed significant negative linear correlations with mid-slope topsoil water content (SWC_{10}) – as did the 'effective' hydraulic conductivity (K_e) in GA. Using SWC_{10}-based values of I_m and F_0 in SVI produced satisfactory to good (NSE > 0.5) predictive results for ~70% of the examined storms, but failed to reproduce hydrographs for six events (23%) with variable runoff responses, possibly because F_0 was also affected by variations in rainfall interception losses between storms. Deviations between calibrated and SWC_{10}-predicted values of F_0 had a greater impact on predicted stormflow amounts than corresponding deviations in I_m.

The median I_m and, to a lesser extent K_e, inferred for the 30 examined events (31.6 and 7.5 mm h^{-1}, respectively) were much higher than the median values of near-surface K_{sat} measurements (2–3 mm h^{-1}, depending on method), confirming the previously suspected under-estimation of field-measured K_{sat} in the study catchment.

Summarizing, using pre-storm topsoil moisture content and 5-min rainfall intensities as the driving variables to model infiltration with a spatially variable infiltration model resulted in more realistic simulated stormflow responses than the classic

Green–Ampt approach or the comparison of rainfall intensities with field-measured K_{sat} to predict stormflow responses at the small catchment scale.

Acknowledgements

Financial support for the fieldwork underlying this study from the China Scholarship Council, VU University Amsterdam, and the Australian Council for International Agricultural Research (ACIAR Grant no. ASEM/2010/050) is gratefully acknowledged. The modeling work by Zhuo Cheng was supported by the National Key Research and Development Program of China (grant no. 2021YFD1500704). We thank the leaders of Barangay Basper for permission to work at Basper, José June Bagay and Roger Tripoli (ACIAR project) for field assistance, Cecille Marie Quiñones (Visayas State University, VSU) for help with field infiltration measurement, and Ofelia Maranguit and Jertz Escala (ACIAR project) for soil physical analysis under supervision of Prof. Angela Ferraren (VSU). Dr. Nestor Gregorio (ACIAR project), Prof. Arturo Pasa (VSU), and Prof. John Herbohn (University of the Sunshine Coast) are thanked for overall facilitation of the field project.

Open Research

The data used for visualization of all figures, the model input data for the 30 examined storm events, and the Python codes employed in the infiltration modeling using GA- and SVI can be accessed via HydroShare: Cheng, Z., J. Zhang (2022). Data_resource_of_figures; Model code_and_input, HydroShare, http://www.hydroshare.org/resource/6a63073f0361493f81e4e48c93fae299

References

Allen RG, Pereira LS, Raes D, Smith M. 1998. Crop evapotranspiration – Guidelines for computing crop water requirements. *FAO Irrigation and Drainage Paper* **56**. UN Food and Agricultural Organization, Rome.

Amoozegar A. 1989. A compact constant-head permeameter for measuring saturated hydraulic conductivity of the vadose zone. *Soil Science Society of America Journal* **53**: 1356–1361.

Arnold JG, Kiniry JR, Srinivasan R, Williams JR, Haney EB, Neitsch SL. 2012. *Soil and Water Assessment Tool Input/Output Documentation Version 2012*. Texas Water Resources Institute Technical Report 436. Texas A & M University, College Station, TX, USA.

Aston AR, Dunin FX. 1979. Coupled infiltration and surface runoff on a 5 ha experimental catchment, Karawarree, N.S.W. *Australian Journal of Soil Research* **17:** 53–64.

Bai ZG, Dent DL, Olsson L, Schaepman ME. 2008. Proxy global assessment of land degradation. *Soil Use and Management* **24**: 223–234.

Beven K. 1989. Changes ideas in hydrology – The case of physically-based models. *Journal of Hydrology* **105**: 157–172.

Birch AL, Stallard RF, Barnard HR. 2021a. Precipitation characteristics and land cover control wet season runoff source and rainfall partitioning in three humid tropical catchments in central Panama. *Water Resources Research* **57**, DOI: 10.1029/2020WR028058

Birch AL, Stallard RF, Bush SA, Barnard HR. 2021b. The influence of land cover and storm magnitude on hydrologic flowpath activation and runoff generation in steep tropical catchments of central Panama. *Journal of Hydrology* **596**, 126138. DOI: 10.1016/j.jhydrol.2021.126138

Birkel C, Correa Barahona A, Duvert C, Granados Bolaños S, Chavarría Palma A, Durán Quesada, Sánchez Murillo R, Bester H. 2021. End Member and Bayesian mixing models consistently indicate near-surface flowpath dominance in a pristine humid tropical rainforest. *Hydrological Processes* **35 (4),** DOI: 10.1002/hyp.14153

Blanchart E, Albrecht A, Brown G, Decaens T, Duboisset A, Lavelle P, Mariani L, Roose E. 2004. Effects of tropical endogeic earthworms on soil erosion. *Agriculture, Ecosystems & Environment* **104**: 303–315.

Blöschl G, Sivapalan M. 1995. Scales issues in hydrological modelling: a review. *Hydrological Processes* **9:** 251–290. DOI:10.1002/hyp.3360090305

Bonell M, Purandara BK, Venkatesh B, Krishnaswamy J, Acharya HAK, Singh UV, Jayakumar R, Chappell NA. 2010. The impact of forest use and reforestation on soil hydraulic conductivity in the Western Ghats of India: implications for surface and sub-surface hydrology. *Journal of Hydrology* **391:** 47–62. DOI:10.1016/j.jhydrol.2010.07.004

Bos MG. 1989. *Discharge measurement structures,* 3rd Ed. *ILRI Publication* 20. International Institute for Land Reclamation and Improvement: Wageningen, the Netherlands, 401 p.

Brooks ES, Boll J, McDaniel PA. 2004. A hillslope-scale experiment to measure lateral saturated hydraulic conductivity. *Water Resources Research* **40, W04208.** DOI: 10.1029/2003WR002858

Bruijnzeel LA. 1988. Estimates of evaporation in plantations of *Agathis dammara* Warb. In South-Central Java, Indonesia. *Journal of Tropical Forest Science* **1**: 145–161.

Bruijnzeel LA. 2004. Hydrological functions of tropical forests: not seeing the soil for the trees? *Agriculture, Ecosystems & Environment* **104**: 185–228. DOI: 10.1016/j.agee.2004.01.015

Brutsaert W. 2005. Infiltration and related unsaturated flows. Chapter 6 in *Hydrology: An introduction*. Cambridge University Press, Cambridge, UK. 307–365.

Bush SA, Stallard RF, Ebel BA, Barnard HR. 2020. Assessing plot-scale impacts of land use on overland flow generation in Central Panama. *Hydrological Processes* **34:** 5043–5069. DOI: 10.1002/hyp.13924

Campos Pinto L, de Mello CR, Norton LD, Poggere GC, Owens PR, Curi N. 2018. A hydropedological approach to a mountainous clayey Humic Dystrudept in the Mantiqueira Range, southeastern Brazil. *Scientia Agricola* **75**: 60–69. DOI: 10.1590/1678-992X-2016-0144

Chandler DG, Walter MF. 1998. Runoff responses among common land uses in the uplands of Matalom, Leyte, Philippines. *Transactions of the American Society of Agricultural Engineers*: **41**: 1635–1641.

Chappell NA, Franks SW, Larenus J. 1998. Multi-scale permeability estimation for a tropical catchment. *Hydrological Processes* **12**: 1507–1523.

Chappell NA, Bonell M, Barnes CJ, Tych W. 2012. Tropical cyclone effects on rapid runoff responses: quantifying with new continuous-time transfer function models. *International Association of Hydrological Sciences Publication* **353:** 82–92.

Chappell NA, McKenna P, Bidin K, Douglas I, Walsh RPD. 1999. Parsimonious modelling of water and suspended-sediment flux from nested-catchments affected by selective tropical forestry. *Philosophical Transactions of the Royal Society (London) Series* **B 354**: 1831–1846.

Chappell NA, Tych W, Chotai A, Bidin K, Sinun W, Thang HC. 2006. BARUMODEL: combined Data Based Mechanistic models of runoff response in a managed rainforest catchment. *Forest Ecology and Management* **224**: 58–80.

Cheng Y, Ogden FL, Zhu J., Bretfeld M. 2018. Land use-dependent preferential flow paths affect hydrological response of steep tropical lowland catchments with saprolitic soils. *Water Resources Research* **54**, WR021875. DOI: 10.1029/2017WR021875

Cinco TA, de Guzman RG, Ortiz AMD, Delfino RJP, Lasco RD, Hilario FD, Juanillo EL, Barba R, Ares, ED. 2016. Observed trends and impacts of tropical cyclones in the Philippines. *International Journal of Climatology* **36**: 4638–4650. DOI: 10.1002/joc.4659

Chu ST. 1978. Infiltration during an unsteady rain. *Water Resources Research* **14:** 461–466.

Concepcion RN, Samar ED. 1995. Grasslands: development attributes, limitations and potentials. In *Strengthening research and development for sustainable management of grasslands*, Bravo MVA, Exconde AB (eds). Forest Research Institute, College: Laguna, The Philippines. 110–116.

Connolly RD, Silburn DM, Ciesiolka CAA. 1997. Distributed parameter hydrology model (ANSWERS) applied to a range of catchment scales using rainfall simulator data. III. Application to a spatially complex catchment. *Journal of Hydrology* **193:** 183–203.

Coughlan KJ. 1997. Description of sites, experimental treatments and methodology. In *A new soil conservation methodology and application to cropping systems in tropical* *steeplands*, Coughlan KJ, Rose CW (eds). ACIAR, Canberra, Australia. 3–8.

Davis SH, Vertessy RA, Silberstein RP. 1999. The sensitivity of a catchment model to soil hydraulic properties obtained by using different measuring techniques. *Hydrological Processes* **13:** 677–688.

Dickinson WT, Whiteley H. 1970. Watershed areas contributing to runoff. *International Association of Hydrological Sciences Publication* **1:** 12–26.

Dubreuil P. 1985. Review of field observations of runoff generation in the tropics. *Journal of Hydrology* **80**: 237–264.

Dunne T, Black RD. 1970. Partial area contributions to storm runoff in a small New England watershed. *Water Resources Research* **6**: 1296–1311.

Dunne T, Zhang WH, Aubry BF. 1991. Effects of rainfall, vegetation, and microtopography on infiltration and runoff. *Water Resources Research* **27:** 2271–2285.

Durán-Zuazo VH, Rodríguez-Pleguezuelo CR. 2008. Soil erosion and runoff prevention by plant covers: a review. *Agronomy for sustainable Development* **28:** 65–86.

Fentie B, Yu B, Silburn MD, Ciesiolka CAA. 2002. Evaluation of eight different methods to predict hillslope runoff rates for a grazing catchment in Australia. *Journal of Hydrology* **261:** 102–114.

Flanagan DC, Ascough II, JC, Nearing MA, Laflen JM. 2001. The water erosion prediction project (WEPP). In *Landscape erosion and evolution modelling*, Harmon RS, Doe III WW (eds). Kluwer Academic Publishers: New York. 145–199.

Garen DC, Moore DS. 2005. Curve Number hydrology in water quality modeling: uses, abuses, and future directions. *Journal of the American Water Resources Association* **41:** 377–388.

Garrity DP, Soekardi M, van Noordwijk M, de la Cruz R, Pathak PS, Gunasena HPM, Van So N, Huijun G, Majid NM. 1997. The *Imperata* grasslands of tropical Asia: area, distribution, and typology. *Agroforestry Systems* **36**: 3–19.

Ghimire CP, Zwartendijk BW, Pde F, Bruijnzeel LA. 2021. Changes in soil hydraulic conductivity and preferential flow pathways after assisted forest restoration on degraded land in the Khasi Hills (Meghalaya, India). Abstract of oral presentation at the EGU General Assembly 2021, EGU 21-6559.

Ghimire CP, Bonell M, Bruijnzeel LA, Coles NA, Lubczynski MW. 2013. Reforesting severely degraded grassland in the Lesser Himalaya of Nepal: effects on soil hydraulic conductivity and overland flow production, *Journal of Geophysical Research: Earth Surface* **118:** 2528–2545. DOI: 10.1002/2013JF002888.

Gibbs HKG, Salmon JM. 2015. Mapping the world's degraded lands. *Applied Geography* **57:** 12–21.

Gupta HV, Sorooshian S, Yapo PO. 1999. Status of automatic calibration for hydrologic models: Comparison with multilevel expert calibration. *Journal of Hydrologic Engineering* **4(2):** 135–143.

Hawkins RH. 1982. Interpretations of source area variability in rainfall-runoff relations. In *Rainfall-runoff relationships*, VP Singh (ed.), Water Resources Publications: Littleton CO, USA. 302–324.

Hawkins RH, Cundy TW. 1987. Steady-state analysis of infiltration and overland flow for spatially-varied hillslopes. *Water Resources Bulletin* **23**: 251–256.

Hewlett JD, Hibbert AR. 1967. Factors affecting the response of small watersheds to precipitation in humid areas. In *International symposium on forest hydrology*, WE Sopper, HW Lull (eds). Pergamon Press: Oxford, UK. 275–290.

James WP, Warinner J, Reedy M. 1992. Application of the Green-Ampt infiltration equation to watershed modeling. *Water Resources Bulletin* **28:** 623–635.

Jasmin BB. 1976. Grassland uses: effect on surface runoff and sediment yield. *SYLVATROP Philippines Forest Research Journal* **1**: 156–172.

Koorevaar P, Menelik G, Dirksen C. 1983. *Elements of soil physics. Developments in Soil Science* **13**. Elsevier Science Ltd: Amsterdam, The Netherlands, 229 p.

Lacombe G, Valentin C, Sounyagong P, de Rouw A, Soulileuth B, Silvera N, Pierret A, Sengthaheuanghoung O, Ribolzi O. 2018. Linking crop structure, throughfall, soil surface conditions, runoff and soil detachment: 10 land uses analyzed in Northern Laos. *Science of the Total Environment* **616–617**: 1330–1338. https://doi.org/10.1016/j.scitotenv.2017.10.185

Lai JB, Ren L. 2007. Assessing the size dependency of measured hydraulic conductivity using double-ring infiltrometers and numerical simulation. *Soil Science Society of America Journal* **71**: 1667–1675. DOI: 10.2136/sssaj2006.0227

Lapides DA, Hahm WJ, Rempe DM, Dietrich WE, Dralle DN. 2022. Controls on streamwater age in a saturation overland flow-dominated catchment. *Water Resources Research* **58**, WR031665. DOI: 10.1029/2021WR031665

Leemhuis C, Erasmi S, Twele A, Kreilein H, Oltchev A, Gerold G. 2007. Rainforest conversion in central Sulawesi, Indonesia: recent development and consequences. *Erdkunde* **61:** 284–293.

Legates DR, McCabe GJ. 1999. Evaluating the use of ‘goodness-of-fit’ measures in hydrologic and hydroclimatic model validation. *Water Resources Research* **35:** 233–241.

Leopoldo PR, de Pádua Sousa A, Filho ST. 1981. Rainfall interception by a sugarcane crop. *Brasil Açcaceiro* **6**: 9–16 (in Portuguese, with abstract in English).

Limsuan MP. 1995. Impacts of grassland use manipulation on water quantity and quality in Angat, Bulacan, Philippines. In *Strengthening research and development for sustainable management of grasslands*, Bravo MVA, Exconde AB (eds). Forest Research Institute: College, Laguna, The Philippines. 136–142.

Liu WJ, Liu W, Lu H, Duan W, Li HM. 2011. Runoff generation in small catchments under a native rainforest and a rubber plantation in Xishuangbanna, southwest China. *Water and Environment Journal* **25:** 138–147. DOI: 10.1111/j.1747-6593.2009.0211.x

Marquardt DW. 1963. An algorithm for least-squares estimation of nonlinear parameters. *Journal of the Society for Industrial and Applied Mathematics* **11**: 431–441.

Martinez LJ, Zinck JA. 2004. Temporal variation of soil compaction and deterioration of soil quality in pasture areas of Colombian Amazonia. *Soil and Tillage Research* **75**: 3–17. DOI: 10.1016/j.still.2002.12.001

Mathys N, Meunier M, Brochot S. 1996. The forest effect on floods in small mountainous catchments: some results from experimental catchments of Draix, France. In *Conference on Ecohydrological Processes in Small Basins*, Strasbourg, France, 24 – 26 September 1996. 123–128.

Mein RG, Larsen CL. 1973. Modeling infiltration during a steady rain. *Water Resources Research* **9:** 384–394.

Mertens J, Madsen H, Kristensen M, Jacques D, Feyen J. 2005. Sensitivity of soil parameters in unsaturated zone modelling and the relation between effective, laboratory and *in situ* estimates. *Hydrological Processes* **19**: 1611–1633. DOI: 10.1002/hyp.5591

Miyata S, Kosugi K, Gomi T, Mizuyama T. 2009. Effects of forest floor coverage on overland flow and soil erosion on hillslopes in Japanese cypress plantation forests. *Water Resources Research* **45**, W06402. https://doi.org/10.1029/2008WR007270

Molina A, Govers G, Vanacker V, Poesen J, Zeelmaekers E, Cisneros F. 2007. Runoff generation in a degraded Andean ecosystem: interaction of vegetation and land use. *Catena* **71**: 357–370. DOI: 10.1016/j.catena.2007.04.002

Nash JE, Sutcliffe JV. 1970. River flow forecasting through conceptual models. Part I – A discussion of principles. Journal of Hydrology **10:** 282–290. DOI: 10.1016/0022-1694(70)90255-6

Nearing MD, Liu BY, Risse LM, Zhang X. 1996. Curve numbers and Green-Ampt effective hydraulic conductivities. *Water Resources Bulletin* **32**: 125–136.

Neitsch SL, Arnold JG, Kiniry JR, Willams JR. 2011. Soil Water Assessment Tool – Theoretical Documentation. Texas Water Resources Institute Technical Report 406. Texas A & M University, College Station, TX, USA.

Obiero JPO. 1996. *Evaluation of infiltration using the Green-Ampt model and rainfall-runoff data for Lagan and Sambret catchments, Kericho, Kenya*. MSc Thesis, University of Nairobi, Nairobi, Kenya, 124 pp.

Ogden FL, Hawkins RP, Walter MT, Goodrich DC. 2017. Comment on “Beyond the SCS-CN method: A theoretical framework for spatially-lumped rainfall-runoff response” by M. S. Bartlett et al. *Water Resources Research.* DOI: 10.1002/2016WR020176

Quiñones CM. 2014. *Properties of soils from ultramafic rocks in the degraded grassland watershed in Basper, Leyte*. MSc Thesis, Visayas State University, Baybay, Leyte Island, the Philippines, 105 p.

Patin J, Mouche E, Ribolzi O, Chaplot V, Sengtahevanghoung O, Latsachak KO, Soulileuth B, Valentin C. 2012. Analysis of runoff production at the plot scale during a long-term survey of a small agricultural catchment in Lao PDR. *Journal of Hydrology* **426–427:** 79–92. DOI: 10.1016/j.jhydrol.2012.01.015

Pirastru M, Bagarello V, Iovino M, Marrosu R, Castellini M, Giadrossich F, Niedda M. 2017. Subsurface flow and large-scale lateral saturated soil hydraulic conductivity in a Mediterranean hillslope with contrasting land uses. *Journal of Hydrology and Hydromechanics* **65:** 297–306. DOI: 10.1515/johh-2017-0006

Ponce VM, Hawkins RH. 1996. Runoff curve number: has it reached maturity? *Journal of Hydrologic Engineering* **1:** 11–19.

Recha JW, Lehmann J, Walter MT, Pell A, Verchot L, Johnson M. 2012. Stream discharge in tropical headwater catchments as a result of forest clearing and soil degradation. *Earth Interactions* **16**–013, DOI:10.1175/2012EI000439.1

Ribolzi O, Evrard, O, Huon S, de Rouw A, Silvera N, Latsachak KO, Soulileuth B, Lefevre I, Pierret A, Lacombe G, Sengtaheuanghoung O, Valentin C. 2017. From shifting cultivation to teak plantation: effects on overland flow and sediment yield in a

montane tropical catchment. *Scientific Reports* **7:3987**. DOI: 10.1038/s41598-017-04385-2
Ribolzi O, Lacombe G, Pierret A, Robain H, Sounyafong P, de Rouw A, Soulileuth B, Mouche E, Huon S, Silvera N, Latsachak KO, Sengtaheuanghoung O, Valentin C. 2018. Interacting land use and soil surface dynamics control groundwater outflow in a montane catchment of the lower Mekong. *Agriculture, Ecosystems & Environment* **268:** 90–102. DOI: 10.1016/j.agee.2018.09.005
Rose CW, Coughlan KJ, Ciesiolka CAA, Fentie B. 1997. The role of soil cover in soil conservation. In *A new soil conservation methodology and application to cropping systems in tropical steeplands*, Coughlan KJ, Rose CW (eds). ACIAR, Canberra, Australia. 59–78.
Shaw EM, Beven KJ, Chappell NA, Lamb R. 2010. *Hydrology in practice*, 4th Ed. CRC Press: Boca Raton FL, USA.
Sharma ML, Barron RJW, Fernie MS. 1987. Areal distribution of infiltration parameters and some soil physical properties in lateritic catchments. *Journal of Hydrology* **94:** 109–127.
Sherlock MD, Chappell NA, McDonnell JJ. 2000. Effects of experimental uncertainty on the calculation of hillslope flow paths. *Hydrological Processes* **14:** 2457–2471.
Shougrakpam S, Sarkar R, Dutta S. 2010. An experimental investigation to characterise soil macroporosity under different land use and land covers of northeast India. *Journal of Earth System Science* **119**: 655–674.
Sidle RC Ziegler AD, Negishi JN, Rahim Nik A, Siew R, Turkelboom F. 2006. Erosion processes in steep terrain – Truths, myths, and uncertainties related to forest management in Southeast Asia. *Forest Ecology & Management* **224**: 199–225. DOI: 10.1016/j.foreco.2005.12.019
Sirimarco X, Barral MP, Villarino SH, Laterra P. 2018. Water regulation by grasslands: a global meta-analysis. *Ecohydrology*, https://doi.org/10.1002/eco.1934
Stone JJ, Paige GB, Hawkins RH. 2008. Rainfall intensity-dependent infiltration rates on rangeland rain-fall simulator plots. *Transactions of the American Society of Agricultural Engineers* **51:** 45–53.
Sutherland RA, Bryan RB. 1990. Runoff and erosion from a small semiarid catchment, Baringo District, Kenya. *Applied Geography* **10:** 91–109.
Taylor CJ, Pedregal DJ, Young PC, Tych W. 2007. Environmental time series analysis and forecasting with the CAPTAIN toolbox. *Environmental Modeling & Software* **22**: 797–814.
Toohey RC, Boll J, Brooks ES, Jones JR. 2018. Effects of land use on soil properties and hydrological processes at the point, plot and catchment scale on volcanic soils near Turrialba, Costa Rica. *Geoderma* **315:** 138–148. DOI: 10.1016/j.geoderma.2017.11.044
USBR. 1997. Water measurement manual, 3rd Ed. US Department of the Interior, bureau of Reclamation, Washington DC. http://www.usbr.gov/tsc/techreferences/mands/wmm/chap07_13.html
Valentin C, Agus F, Alamban R, Boosaner A, Bricquet JP and 14 others. 2008. Runoff and sediment losses from 27 upland catchments in Southeast Asia: impacts of rapid land

use changes and conservation practices. *Agriculture, Ecosystems & Environment* **128**: 225–238. DOI: 10.1016/j.agee.2008.06.004

Van Dijk AIJM, Bruijnzeel LA. 2004. Runoff and soil loss from bench terraces. 1. An event-based model of rainfall infiltration and surface runoff. *European Journal of Soil Science* **55:** 299–316. DOI: 10.1111/j.1365-2389.2004.00604.x

Van Meerveld HJ, Zhang J, Tripoli R, Bruijnzeel LA. 2019. Effect of reforestation of a degraded *Imperata* grassland on dominant flow pathways and streamflow responses in Leyte, the Philippines. *Water Resources Research* **55**, DOI: 10.1029/2018WR023896

Van Mullem JA. 1991. Runoff and peak discharges using Green-Ampt infiltration model. *Journal of Hydrologic Engineering* **117:** 354–370.

Waterloo MJ, Bruijnzeel LA, Vugts HJ, Rawaq TT. 1999. Evaporation from Pinus caribaea plantations on former grassland soils under maritime tropical conditions. *Water Resources Research* **35:** 2133–2144.

Wen X, Gomez-Hernandez JJ. 1996. Upscaling hydraulic conductivities in heterogeneous media: A review. *Journal of Hydrology* **183:** 9-32.

White JT, Hunt RJ, Fienen MN, Doherty JE. 2020. Approaches to highly parameterized inversion: PEST++ Version 5, a Software suite for parameter estimation, uncertainty analysis, management optimization and sensitivity analysis. *US Geological Survey Techniques and Methods* **7C26**, 52 p. https://pubs.er.usgs.gov/publication/tm7C26

Wiersum KF. 1985. Effects of various vegetation layers in an *Acacia auriculiformis* forest plantation on surface erosion in Java, Indonesia. In: *Soil Erosion and Conservation*, El-Swaify S, Moldenhauer WC, Lo A. (Eds.). Soil Conservation Society of America: Ankeny, Wisconsin, pp. 79–89.

Yamamoto, EMS, Sayama T, Yamamoto K, Apip A. 2020. Comparison of runoff generation methods for land use impact assessment using the SWAT model in humid tropics. *Hydrological Research Letters* **14**: 81–88. DOI: 10.3178/hrl.14.81

Yin J, Gentine P, Zhou S, Sullivan SC, Wang R, Zhang Y, Guo SL. 2019. Large increase in global runoff extremes driven by climate and anthropogenic changes. *Nature Communications* (2018) **9**:4389. DOI: 10.1038/s41467-018-06765-2

Yira Y, Diekkrüger B, Steup G, Bossa AY. 2016. Modeling land use change impacts on water resources in a tropical West African catchment (Dano, Burkina Faso). *Journal of Hydrology* **537:** 187–199. DOI: 10.1016/j.jhydrol.2016.03.052

Young PC. 2001. Data-Based Mechanistic modelling and validation of rainfall–flow processes. In *Model validation: perspectives in hydrological science*, Anderson MG, Bates PG (eds). Wiley & Sons: Chichester, UK. 117–161.

Yu B. 1999. A comparison of the Green–Ampt and a spatially variable infiltration model for natural storm events. *Transactions of the American Society of Agricultural Engineering* **42:** 89–97.

Yu B. 2005. Process-based erosion modelling: promises and progress. In *Forests, water and people in the humid tropics*, Bonell M, Bruijnzeel LA (eds). Cambridge University Press: Cambridge, UK. 790–810.

Yu B. 2012. Validation of SCS method for runoff estimation. *Journal of Hydrologic Engineering* **2012.17:** 1158–1163.

Yu B, Rose CW, Coughlan FJ, Fentie B. 1997a. Plot-scale rainfall-runoff characteristics and modelling at six sites in Australia and South East Asia. *Transactions of the American Society of Agricultural Engineering* **40**: 1295–1303.

Yu B, Rose CW, Coughlan KJ, Fentie B. 1997b. Plot-scale runoff modelling for soil loss prediction. In In *A new soil conservation methodology and application to cropping systems in tropical steeplands*, Coughlan KJ, Rose CW (eds). ACIAR, Canberra, Australia. 24–33.

Yu B, Rose CW, Ciesiolka CCA, Cakurs U. 2000. The relationship between runoff rate and lag time and the effects of surface treatments at the plot scale. *Hydrological Sciences Journal* **45:** 709–726.

Yu B, Sombatanit S, Rose CW, Ciesiolka CAA, Coughlan KJ. 2000. Characteristics and modeling of runoff hydrographs for different tillage treatments. *Soil Science Society of America Journal* **64:** 1763–1770.

Zehe E, Flühler W. 2001. Slope-scale variation of flow patterns in soil profiles. *Journal of Hydrology* **247:** 116–132. DOI: 10.1016/S0022-1694(01)00371-7

Zhang J, van Meerveld HJ, Tripoli, R, Bruijnzeel LA. 2018a. Runoff response and sediment yield of a landslide-affected fire-climax grassland catchment (Leyte, The Philippines) before and after passage of typhoon Haiyan. *Journal of Hydrology* **565:** 524–537. DOI: 10.1016/j.jhydrol.2018.08.016

Zhang J, Bruijnzeel LA, Tripoli R, van Meerveld HJ. 2018b. Water budget and run-off response of a tropical multispecies "reforest" and effects of typhoon disturbance. *Ecohydrology* 2018; e2055. https://doi.org/10.1002/eco.2055

Zhang J, Bruijnzeel LA, Quiñones MC, Tripoli R, Asio VB, van Meerveld HJ. 2019a. Comparative soil physical characteristics of a fire-climax grassland and a multi-species reforest (Leyte, the Philippines): implications for runoff generation. *Geoderma* **333:** 163–177. DOI: 10.1016/j.geoderma.2018.07.022

Zhang J, Tych W, Chappell N, van Meerveld HJ, Bruijnzeel LA. 2019b. Separating effects of rainfall variability and typhoon disturbance on the runoff response of a tropical 'reforest' using a data-based mechanistic modeling approach. Abstract EGU2019-10222. Annual Assembly of the European Geophysical Union, Vienna, April 2019.

Ziegler AD, Giambelluca TW, Tran LT, Vana TT, Nullet MA, Fox J, Vien TD, Pinthong J, Maxwell JF, Evett S. 2004. Hydrological consequences of landscape fragmentation in mountainous northern Vietnam: evidence of accelerated overland flow generation. *Journal of Hydrology* **287**: 124–146. DOI: 10.1016/j.jhydrol.2003.09.027

Ziegler AD, Bruun TB, Guardiola-Claramonte M, Giambelluca TW, Lawrence D, Thanh Lam N. 2009. Environmental consequences of the demise in swidden cultivation in montane mainland Southeast Asia: hydrology and geomorphology. *Human Ecology* **37**: 361–373. DOI: 10.1007/s10745-009-9258-x

Zimmermann B, Elsenbeer H, De Moraes JM. 2006. The influence of land-use changes on soil hydraulic properties: implications for runoff generation. *Forest Ecology and Management* **222**: 29–38. DOI: 10.1016/j.foreco.2005.10.070

Zwartendijk BW, van Meerveld HJ, Ghimire CP, Bruijnzeel LA, Ravelona M, Jones JPG.

2017. Rebuilding soil hydrological functioning after swidden agriculture in eastern Madagascar. *Agriculture, Ecosystems & Environment* **239**: 101–111. DOI: 10.1016/j.agee.2017.01.002

References From the Supporting Information

Bonell M, Barnes CJ, Grant CR, Howard A, Burns J. 1998. High rainfall, response-dominated catchments: a comparative study of experiments in tropical northeast Queensland with temperate New Zealand. In: *Isotope tracers in catchment hydrology*, Kendall C, McDonnell JJ (Eds.). Elsevier, Amsterdam, 347–390.

*Chappell NA, Bonell M, Barnes CJ, Tych W. 2012. Tropical cyclone effects on rapid runoff responses: quantifying with new continuous-time transfer function models. *International Association of Hydrological Sciences Publication* **353:** 82–92.

*Chappell NA, McKenna P, Bidin K, Douglas I, Walsh RPD. 1999. Parsimonious modelling of water and suspended-sediment flux from nested-catchments affected by selective tropical forestry. *Philosophical Transactions of the Royal Society (London) Series* **B 354**: 1831–1846.

*Coughlan KJ. 1997. Description of sites, experimental treatments and methodology. In *A new soil conservation methodology and application to cropping systems in tropical steeplands*, Coughlan KJ, Rose CW (eds). ACIAR, Canberra, Australia. 3–8.

*Van Dijk AIJM, Bruijnzeel LA. 2004. Runoff and soil loss from bench terraces. 1. An event-based model of rainfall infiltration and surface runoff. *European Journal of Soil Science* **55:** 299–316. DOI: 10.1111/j.1365-2389.2004.00604.x

*Yu B, Rose CW, Coughlan KJ, Fentie B. 1997b. Plot-scale runoff modelling for soil loss prediction. In In *A new soil conservation methodology and application to cropping systems in tropical steeplands*, Coughlan KJ, Rose CW (eds). ACIAR, Canberra, Australia. 24–33.

*Note:*references from the supporting information have been listed in the main reference list.*

Water Resources Research

Supporting Information for

Stormflow response and 'effective' hydraulic conductivity of a degraded tropical *Imperata* grassland catchment as evaluated with two infiltration models

Zhuo Cheng[1,2], Jun Zhang[3,4,*], Bofu Yu[2], Nick A. Chappell[5],

H.J. (Ilja) van Meerveld[6], and L. Adrian Bruijnzeel[3,7]

[1]Department of Geography, Beijing Normal University, Beijing, P. R. China

[2]Australian Rivers Institute and School of Engineering and Built Environment, Griffith University, Brisbane, Australia

[3]Institute of International Rivers and Eco-Security, Yunnan University, Kunming, P. R. China

[4]Environmental Modelling, Sensing & Analysis, TNO, Petten, The Netherlands

[5]Lancaster Environment Centre, University of Lancaster, Lancaster, United Kingdom

[6]Department of Geography, Hydrology and Climate, University of Zurich, Zurich, Switzerland

[7]Department of Geography, King's College London, London, United Kingdom

Contents of this file

Introduction

Supporting text S1 provides additional evidence regarding the dominance of infiltration-excess overland flow at the study site. Supporting Figure S1 graphically illustrates the conceptual difference between the two infiltration models employed in the study (GA and SVI) whereas Supporting Figures S2–S4 present additional examples of the comparative performance of the GA and SVI models for different types of storm events. The remaining Supporting Figures present the temporal variability of the spatially averaged maximum infiltration parameter I_m in the SVI model (S5) as well as tentative relations between I_m (and initial abstraction loss, F_0) and soil bulk density / soil organic matter content (S6) or the 'effective' hydraulic conductivity in the GA model (S7).

Text S1.

Data-Based Mechanistic model application and evidence for stormflow runoff generation regime

The 157-mm rain event on 28–29 June 2013 produced a very flashy streamflow generation with a transfer time ('time constant') of the propagating flood wave (*i.e.,* celerities) through the catchment of 84 min. For this period in this catchment, the optimal model producing this time constant is a purely first-order linear model with no delay between rainfall and first streamflow response and a Nash-Sutcliffe simulation efficiency of 0.90. The rainfall to riparian pore-water response (regulated by a subsurface response) for this event was, however, considerably slower with a response time of 59 hours plus 5 min delay; this also had a first-order linear transfer function structure. An even more flashy time of response of only 16 min was produced for the smaller 55 mm event over the 3–5 July 2013 period. The optimal model structure identified was the same as for the 28–29 June event, though the simulation efficiency was lower (0.81). Again, the response of the riparian pore-water level to rainfall was considerably slower at 417 hours plus 40 min delay between rainfall and initial piezometer response (Rt^2 0.90). The observations also demonstrated that streamflow peaked well before the riparian water-level (as observed in the piezometer) reached the ground surface. This observation, combined with the systems modeling, indicates that both periods (and others examined in the record), exhibit a response of the riparian subsurface that is considerably slower / more damped when compared with the streamflow, indicating that infiltration-excess overland flow is the dominant source of streamflow for these events at this locality. Indeed, the response time of only 16 min for the July storm is considerably more flashy than that observed for the similarly-sized South Creek Experimental Catchment in Queensland during the severe Category 4 Tropical Cyclone Joy (Chappell *et al.,* 2012), where saturation overland flow on the hillside was considered a dominant pathway (Bonell *et al.,* 1998).

Datasets	Period	Structure1	a[2]	b[3]	Rt^2 [4]	YIC5	TC6
Rain-streamflow	28-29/6/2013	[1 1 0]	-0.9423	0.0263	0.90052	-4.272	84.07 min
Rain-streamflow	3-5/7/2013	[1 1 1]	-0.7419	0.0897	0.81209	-6.396	16.75 min
Rain-porewater	28-29/6/2013	[1 1 1]	-0.9986	0.6049	0.92218	-6.496	59.28 hours
Rain-porewater	3-5/7/2013	[1 1 8]	-0.9998	0.7128	0.90420	-9.978	417.10 hours

[1] transfer function model structure given in form of [number of denominators; number of numerators; number of pure time delays];

[2] The value of the 'a' or recession parameter identified for a first-order discrete time transfer function model;

[3] The value of the 'b' or gain parameter identified for a first-order discrete time transfer function model;

[4] Simplified Nash-Sutcliffe simulation efficiency (R_t^2);

[5] Young Information Criterion (YIC);

[6] Time constant of the identified first-order, discrete-time transfer function model derived from the 'a' parameter and data time-step. See Chappell *et al.* (1999) for explanations.

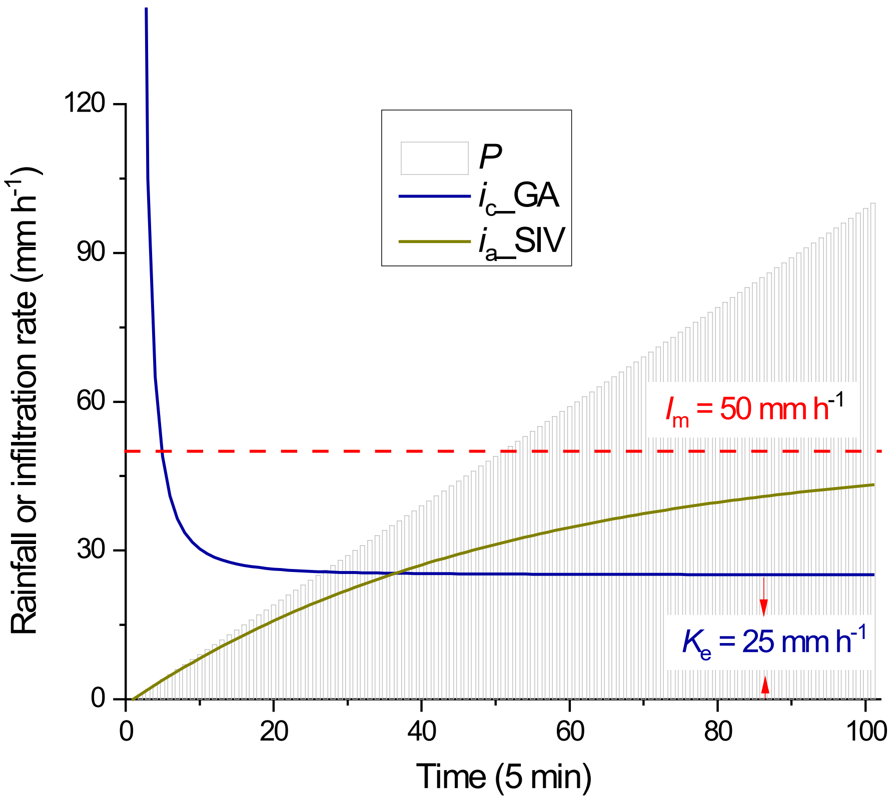

Figure S1. Illustration of the different ways in which the infiltration process is modeled by the GA and SVI models for an event with a linearly increasing rainfall intensity: i_c_GA is the infiltration capacity as derived by GA for K_e= 25 mm h^{-1} and ψ_m = 0.8 mm; i_a_SVI denotes the actual infiltration rate according to SVI for F_0 =10 mm and I_m = 50 mm h^{-1}.

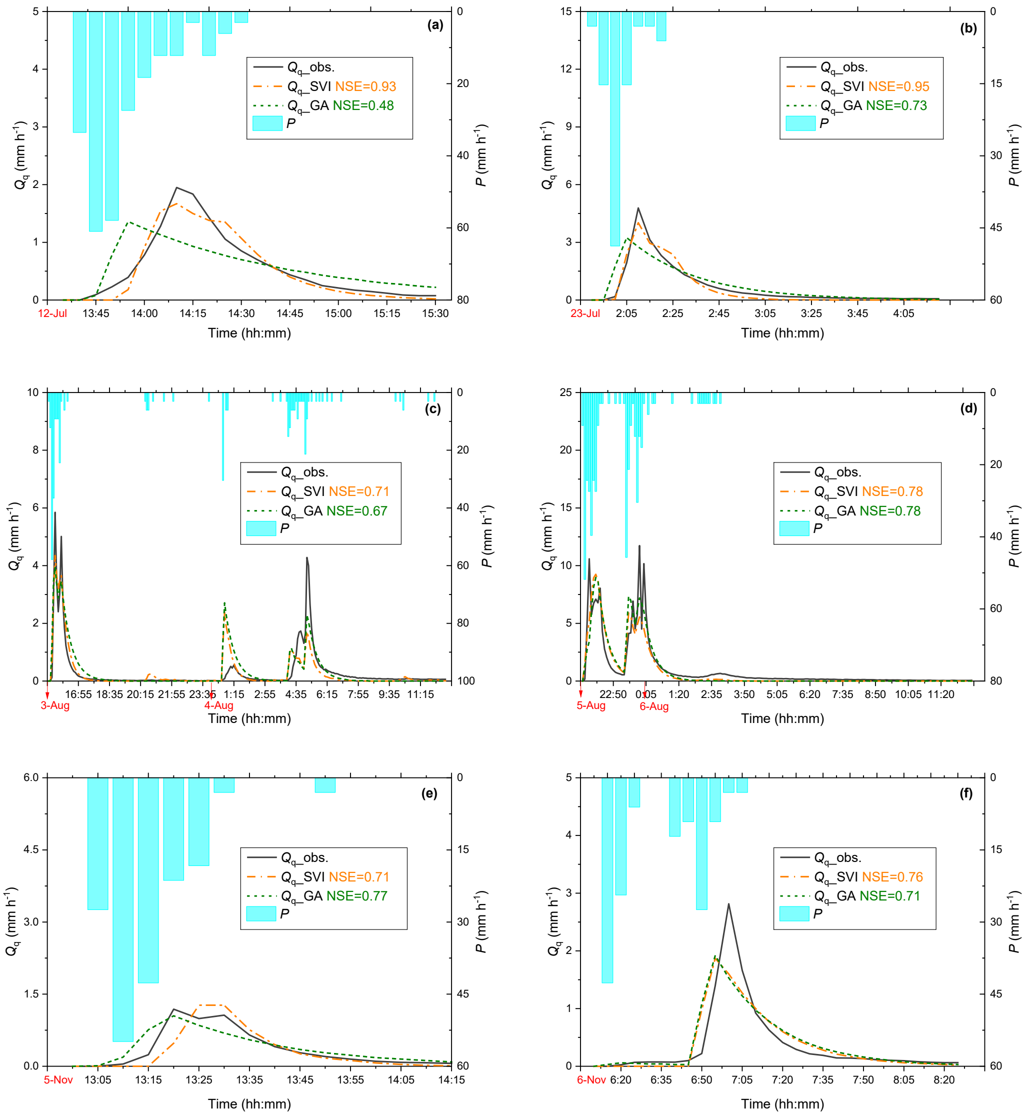

Figure S2. Comparison of observed and predicted hydrographs by GA and SVI for selected storm events. NSE = Nash-Sutcliffe efficiency value.

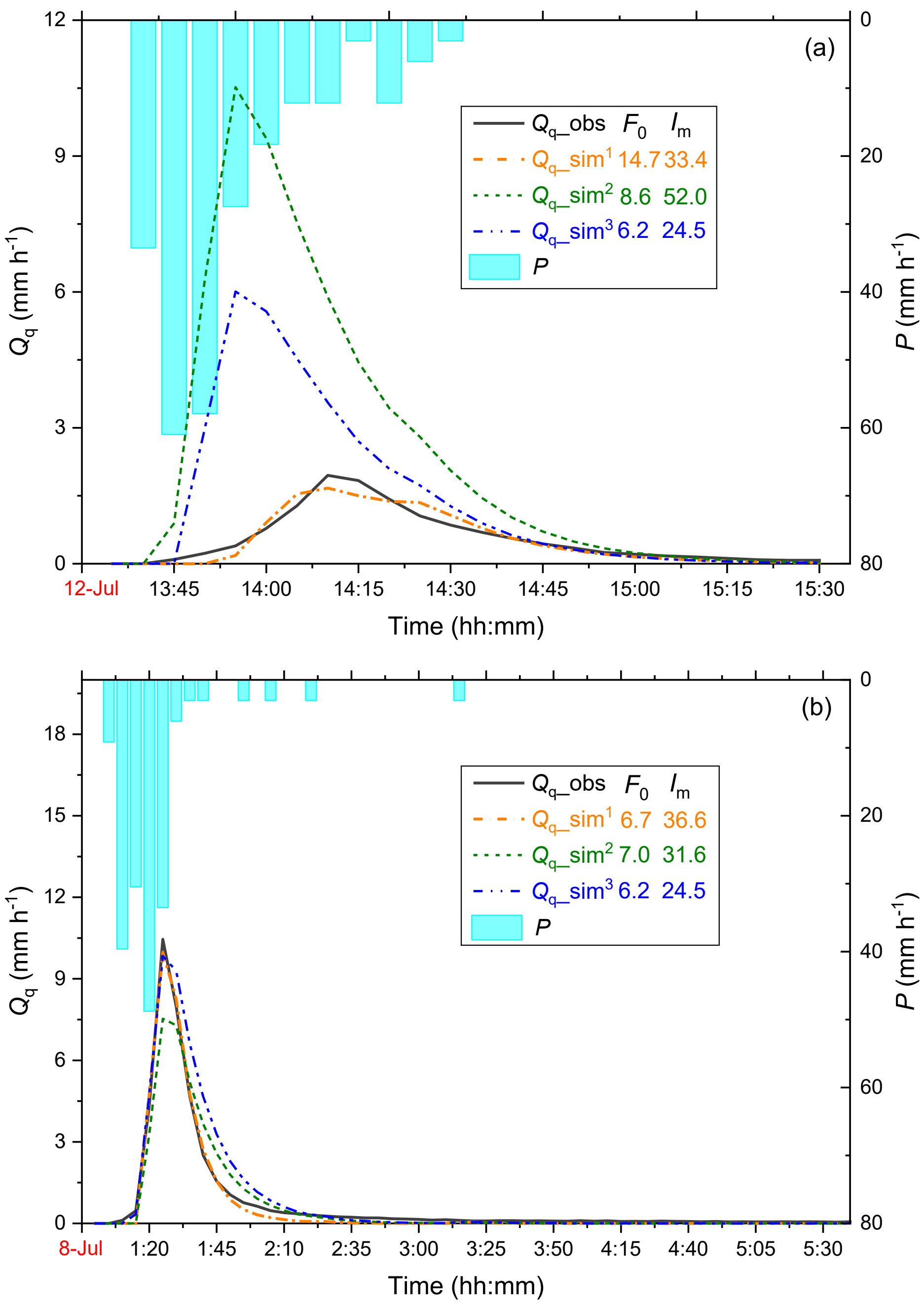

Figure S3. Comparison of observed (Q_q_obs) and predicted (Q_{q_sim}) hydrographs by SVI in three modes, *i.e.* with both parameters calibrated (Q_q_sim^1); with median values of calibrated parameters for all 30 events (Q_q_sim^2); and with parameters derived from SWC_{10}. Panel **(a)** represents the highest discrepancy in performance for the three predictions (event of 12 July 2013, 20.6 mm of rain, storm runoff coefficient (R_c) of 5%), and panel **(b)** the lowest discrepancy (event of 8 July 2013, 15.5 mm, R_c = 21%).

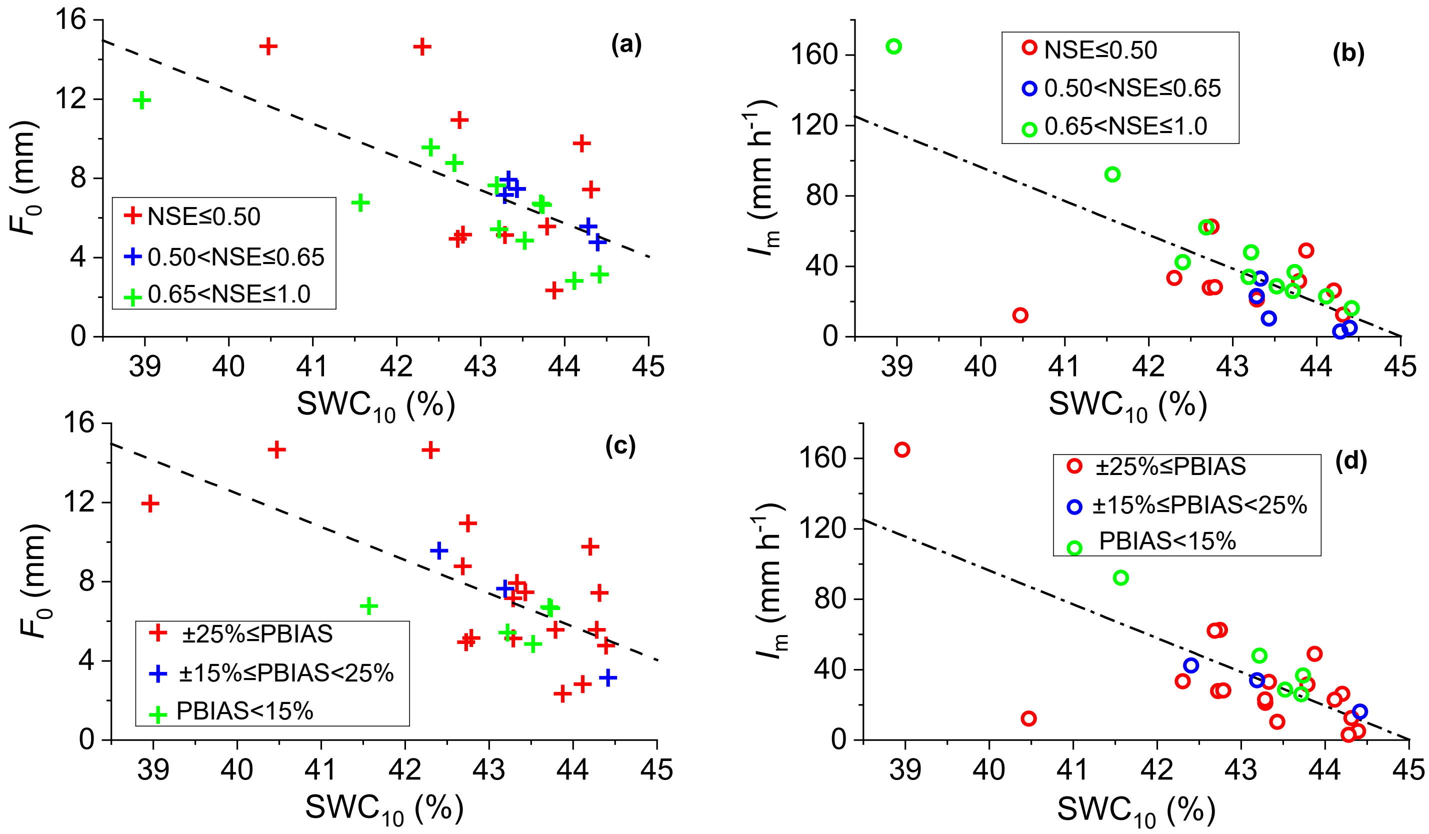

Figure S4. Relations between mid-slope soil moisture content at 10 cm (SWC$_{10}$) and the calibrated values of initial abstraction, F_0 and the spatially average maximum infiltration capacity, I_m for 26 events; points are colour-coded by the class of **(a) & (b)** Nash-Sutcliffe efficiency, NSE and **(c) & (d)** the ratio of the simulated to the observed event total stormflow (PBIAS) for the simulations using predicted values of F_0 and I_m (dashed lines).

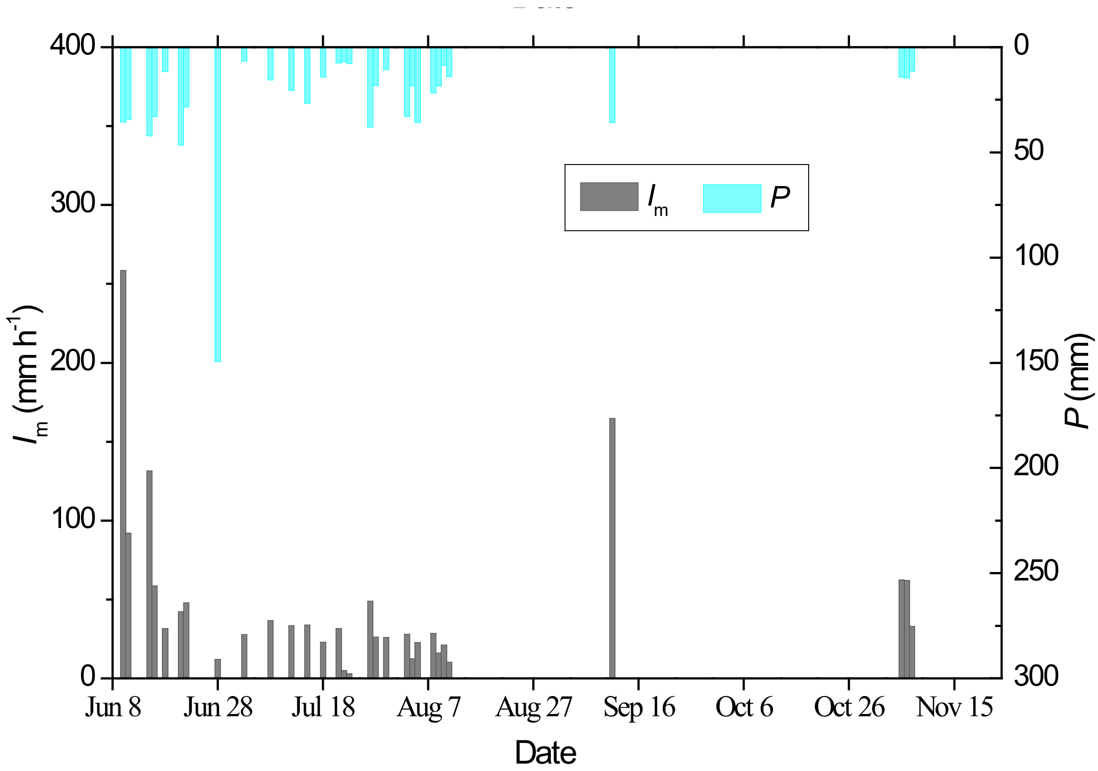

Figure S5. Temporal variability of the spatially averaged maximum infiltration capacity I_m as derived for each individual runoff event between 8 June and 7 November 2013.

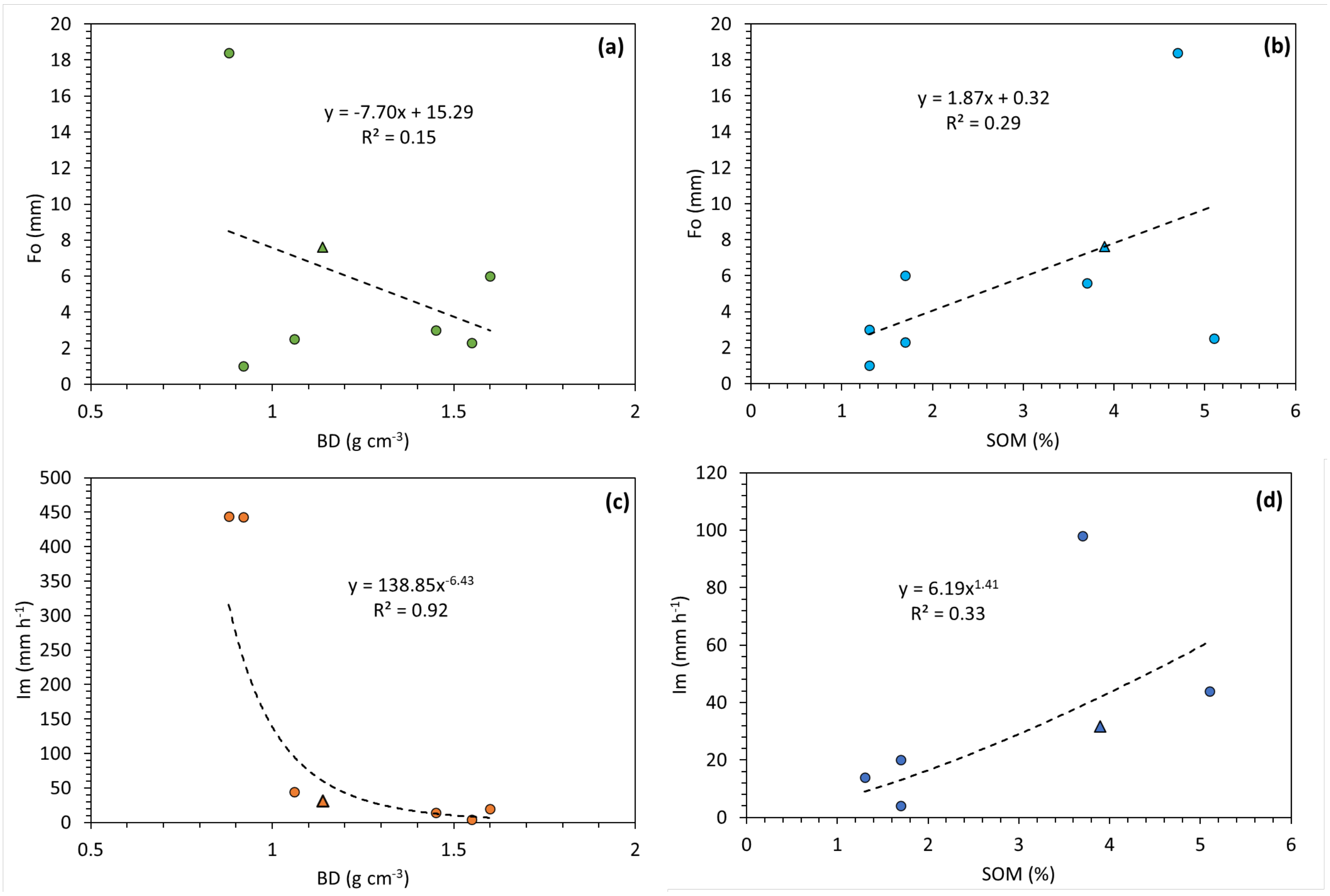

Figure S6. Tentative relationships between **(a)** soil bulk density (BD, g cm^{-3}) and **(b)** soil organic matter content (SOM, %) and initial abstraction, F_0 (mm); and between **(c)** BD and **(d)** SOM and the spatially averaged maximum infiltration rate (I_m, mm h^{-1}) as measured at various sites in Southeast Asia (Yu *et al.*, 1997b; Coughlan, 1997; Van Dijk & Bruijnzeel, 2004). Data for the Basper grassland indicated by triangle.

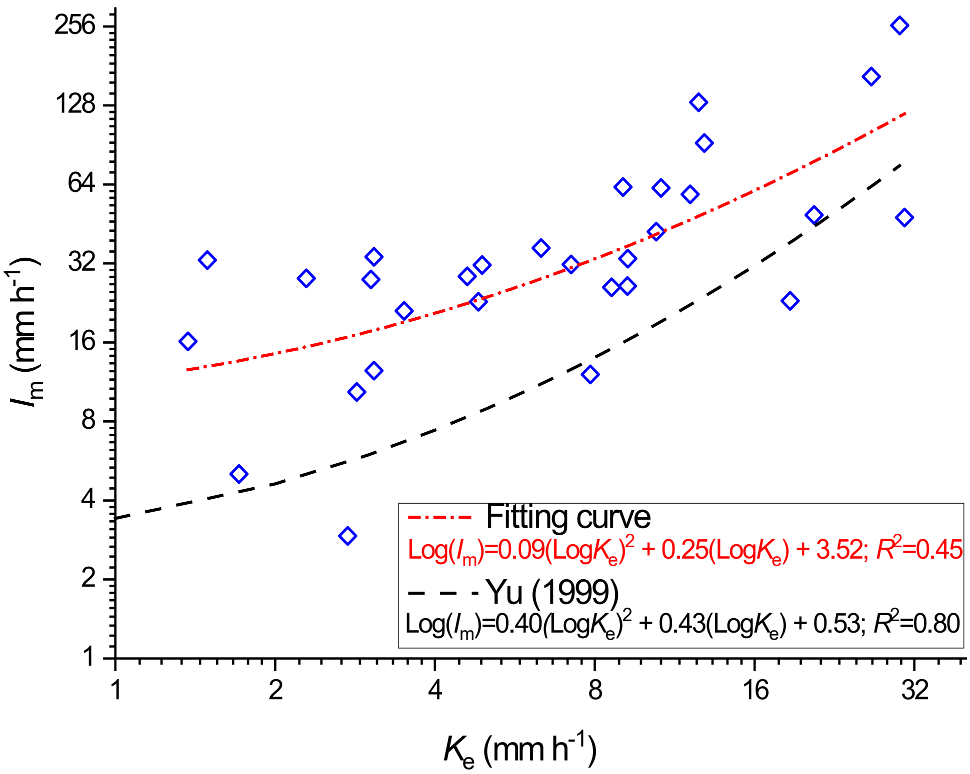

Figure S7. Relationship between Log(I_m)- and Log(K_e)-values derived for each of the 30 examined runoff events at the Basper grassland. Second-order polynomial equation derived by Yu (1999) for six sites in Southeast Asia and Queensland added for comparison.